
PERMUTAION EQUIVARIANT GRAPH FRAMELETS FOR HETEROGENEOUS SEMI-SUPERVISED LEARNING

Jianfei Li* *

Ruigang Zheng*†

Han Feng‡

Xiaosheng Zhuang§

June 8, 2023

ABSTRACT

The nature of heterophilous graphs is significantly different with that of homophilous graphs, which suggests aggregations beyond 1-hop neighborhood and causes difficulties in early graph neural network models. In this paper, we develop a new way to implement multi-scale extraction via constructing Haar-type graph framelets with desired properties of permutation equivariance, efficiency, and sparsity, for deep learning tasks on graphs. We further design a graph framelet neural network model PEGFAN using our constructed graph framelets. The experiments are conducted on a synthetic dataset and 9 benchmark datasets to compare performance with other state-of-the-art models. The result shows that our model can achieve best performance on certain datasets of heterophilous graphs (including the majority of heterophilous datasets with relatively larger sizes and denser connections) and competitive performance on the remaining.

1 Introduction

Graphs are ubiquitous data structures for a variety of real-life entities, such as traffic networks, social networks, citation networks, chemo- and bio-informatics networks, etc. With the abstraction via graphs, many real-life problems that are related to networks and communities can be cast into a unified framework and solved by exploiting its underlying rich and deep mathematical theory as well as tremendously efficient computational techniques. In recent years, graph neural networks (GNNs) for graph learning such as node classification [16], link prediction [31], and graph classification [32], have demonstrated their powerful learning ability and achieved remarkable performance [35]. In the particular field of node classification, many GNN models follow the *homophily* assumption, that is, the majority of edges connect nodes from the same classes (e.g., researchers in a citation network tend to cite each other from the same area), yet graphs with *heterophily*, that is, the majority of edges connect nodes from different classes [33], do exist in many real-world scenarios. A typical example is in a cyber network, a phishing attacker usually sends fraudulent messages to a large population of normal users (victims) in order to obtain sensitive information. We refer to [19, 25] for the limitations of early GNNs on homophilous graphs and a recent survey paper [33] on GNNs for heterophilous graphs.

Heterophilous graphs differ from homophilous graphs not only *spatially* in terms of distribution beyond the 1-hop neighborhood but also *spectrally* with larger oscillation in terms of the frequency distribution of graph signals under the graph Laplacian. Such properties bring challenges to learning on heterophilous graphs and demand new GNNs the ability to extract intrinsic information in order to achieve high performance. To enhance the influence of nodes from the same classes that are outside of 1-hop neighborhoods, one common approach is based on the *multi-hop aggregation* to leverage information of k -hop neighborhoods, $k \geq 2$. Its effectiveness for heterophilous graphs is emphasized and theoretically verified in [36]. A common way to perform multi-hop aggregation is to utilize the powers of the adjacency matrix. However, the use of higher powers of adjacency matrix will result in a convergent phenomenon as shown in [19] and may fail to capture meaningful information. Moreover, they may lead to dense matrices and cause computation

*Department of Mathematics, City University of Hong Kong (jianfeili2-c@my.cityu.edu.hk)

†Department of Mathematics, City University of Hong Kong (ruigzheng2-c@my.cityu.edu.hk)

‡Department of Mathematics, City University of Hong Kong (hanfeng@cityu.edu.hk)

§Department of Mathematics, City University of Hong Kong (xzhuang7@cityu.edu.hk)

*Equal contribution.

and storage burdens. To seek further improvement, it is thus natural to consider an alternative spatial resolution of graphs other than k -hop neighborhood. To answer this question, we work on the theory of wavelet/framelet systems on graphs which brings a notion of *scale* on graphs and wavelets/framelets corresponding to such scales. In this paper, we introduce and integrate a dedicated graph framelet system so as to perform *multi-scale extraction* on graphs.

Actually, classical wavelets/framelets in the Euclidean domains [8, 14] are well-known examples of multi-scale representation, which have been extended to irregular domains such as graphs and manifolds under similar principles in recent years, e.g., see [13, 5, 10, 17]. Some graph wavelets/framelets systems are also proposed and applied in GNNs for node and graph classifications [18, 28, 34]. When the graph is reordered, it is natural to expect the produced wavelets/framelets to be reordered in the same way for robust learning. However, most of the graph wavelets/framelets do not possess such a property of *permutation equivariance*. That is, up to certain permutations, the constructed graph wavelet/framelet systems should be the “same” regardless of the underlying node orderings. The work on Haar-type graph wavelets/framelets [11, 5, 6, 18, 29] are “piecewise-constant” functions on graphs that depend on a given tree with certain underlying node ordering. If new orderings are given, though the underlying graph and graph data are the same, the newly resulted graph wavelets/framelets are no longer the same. Without the property of permutation equivariance, the network outputs could vary with respect to graph reordering and thus lead to instability of the GNNs.

In this paper, we provide a novel and general method to construct Haar-type graph framelets having the permutation equivariance property, which further implies the permutation equivariance of our graph framelet neural network model PEGFAN (Permutation Equivariant Graph Framelet Augmented Network). Our Haar-type graph framelets are constructed spatially with respect to a hierarchical structure on the underlying graph. Scales in such systems correspond to the levels in the hierarchical structure in which higher levels are associated with larger groups of nodes. Multi-scale extractions via such graph framelets are regarded as alternatives and supplements for the usual multi-hop aggregations. Moreover, we show that our graph framelets possess sparse representation property, which leads to the sparsity property of the orthogonal projection matrix (framelet matrix) formed by stacking those framelet vectors at certain scales. This is in contrast to the high powers of adjacency matrices and their non-sparse nature. Furthermore, we apply our graph framelets in the neural network architecture design by using the framelet matrices at different scales as well as the adjacency matrices to form multi-channel input and perform multi-scale extraction through attention and concatenation. The state-of-the-art node classification accuracies on several benchmark datasets validate the effectiveness of our GFNN model.

In summary, the contribution of this paper is as follows: 1) We propose a novel and general method to construct Haar-type graph framelets that have properties of permutation equivariance, sparse representation, efficient computation, and so on. 2) We apply our Haar-type graph framelet system to extract multi-scale information and integrate it into a graph neural network architecture 3) We demonstrate the effectiveness of our model for node classification on synthetic and benchmark datasets via extensive comparisons with several state-of-the-art GNN models.

2 Related Work

Early work on node classification includes [9, 16, 12], which are some of the earliest examples of spectral and spatial GNNs. [26] is the first article that aims at heterophilous graphs. [33] provides a comprehensive review of graph neural networks for graphs with heterophily.

Multi-hop Aggregation in GNNs Papers of [30, 1, 36, 23] are GNNs that adopt hidden layer concatenation and multi-hop aggregation and involve the powers of adjacency matrices. Thus, they resemble each other in terms of neural network architecture. The difference is that [30, 1] mainly deal with homophilous datasets. On the other hand, with emphasis on the heterophilous setting, [36] theoretically shows the importance of concatenation of aggregation beyond the 1-hop neighborhood, with an addition on the importance of ego- and neighbor-embedding separation. Such non-local neighborhood aggregation is also emphasized in [12, 30]. The current state-of-the-art model FSGNN, i.e., Feature Selection GNN [23], is different from the previous ones by, in our interpretation, viewing the semi-supervised setting as a supervised setting in which multi-hop aggregation is regarded as input of different feature channels from different hops and were not applied in the following layers. As a result, its network architecture basically consists of a *mix-hop* [1] layer and fully-connected layers with attention weights for different channels being applied before the concatenation. It is worth mentioning that a recent work [20] on large-scale heterophilous node classification is very similar to [23], in which input channels were limited to the 0-hop and the 1-hop.

Graph Wavelets/Framelets Papers of [7, 11, 13, 5, 10, 6, 18, 29] are work of graph wavelets/framelets in which [13, 10] is spectral-type and the rest are Haar-type. A framelet system differs from the classical (orthogonal) wavelet system by being a frame in a Hilbert space and offering redundant representation. The Haar-type wavelet system in [7] is defined for different nodes as centers. [11, 5, 6, 18, 29] define graph wavelets/framelets under a given tree and they differ in the interpretation and generation of the tree. [11] applies to trees from graphs. In [5], the tree is represented as

a filtration on $[0, 1]$, and the wavelet system is equivalent to an orthogonal basis of tree polynomials. Similar to [5], the trees are further generalized to hierarchical partitions of $[0, 1]^2$ in [6] and apply to directed graphs, and a Haar-type wavelet system for directed graphs is thus constructed. [29] further generalizes the work in [6, 15] by considering the constructions of Haar-type framelet systems on any compact sets in \mathbb{R}^d under a given hierarchical partition and adapt the construction of directed graph framelets to such cases.

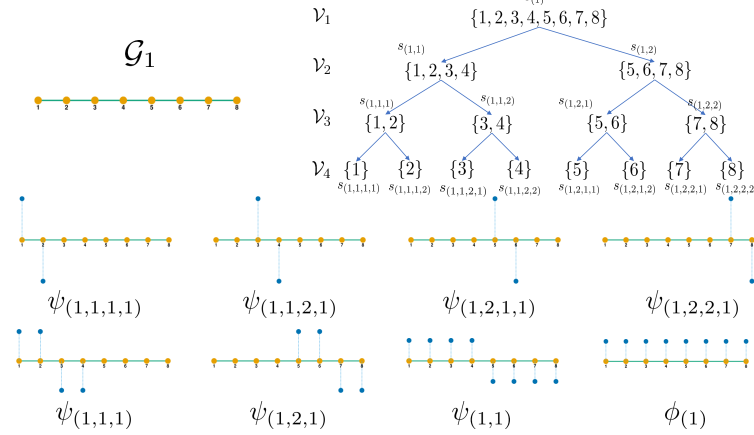


Figure 1: Graph framelets w.r.t. \mathcal{G}_1 (top-left) and the hierarchical partition $\mathcal{P}_4 = \{\mathcal{V}_1, \mathcal{V}_2, \mathcal{V}_3, \mathcal{V}_4\}$ (top-right). The height of blue points represents the value of graph framelets ψ_Λ (bottom 8), and they are above the graph if values are positive, and below otherwise. $\phi_{(1)}$ is the scaling vector at the coarsest level.

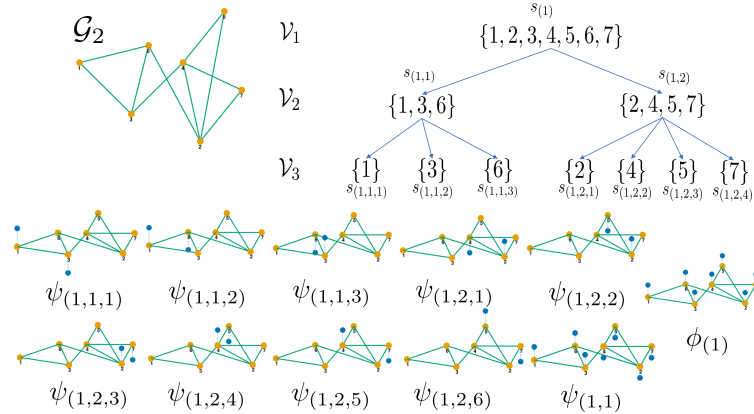


Figure 2: Graph framelets ψ_Λ w.r.t. \mathcal{G}_2 and the hierarchical partition $\mathcal{P}_3 = \{\mathcal{V}_1, \mathcal{V}_2, \mathcal{V}_3\}$. See also Figure 1.

3 Permutation Equivariant Graph Framelets

In this section, we develop permutation equivariant graph framelet systems with properties of sparsity, efficiency, and permutation equivariance, which yield robustness and effective algorithms for the GFNN model. The proofs of the main results in this section can be found in Appendix A.

3.1 Preliminaries

Let $\mathcal{G} = (\mathcal{V}, \mathcal{E})$ be a graph, where $\mathcal{V} = \{v_1, \dots, v_n\}$ is the vertex set containing n vertices (or equivalently, we simply identify $\mathcal{V} = \{1, 2, \dots, n\}$), and $\mathcal{E} \subset \mathcal{V} \times \mathcal{V}$ is the edge set of ordered pairs (i, j) . The adjacency matrix $\mathbf{A} : \mathcal{V} \times \mathcal{V} \rightarrow \mathbb{R}$ of \mathcal{G} is a matrix of size $n \times n$ such that its (i, j) -entry a_{ij} is the weight on edge (i, j) and $a_{ij} = 0$ if $(i, j) \notin \mathcal{E}$. We denote $\tilde{\mathbf{A}} := \mathbf{D}^{-1/2} \mathbf{A} \mathbf{D}^{-1/2}$ with \mathbf{D} being the diagonal degree matrix of \mathcal{G} . A signal \mathbf{f} on the graph is defined as

$\mathbf{f} : \mathcal{V} \rightarrow \mathbb{R}$ with ℓ_2 norm $\|\mathbf{f}\|^2 = \sum_{i=1}^n f_i^2 < \infty$. All such ℓ_2 signals on \mathcal{G} forms a Hilbert space $L_2(\mathcal{G})$. A collection $\{\mathbf{e}_m : m \in [M]\} \subset L_2(\mathcal{G})$ is a *tight frame* of $L_2(\mathcal{G})$ if $\mathbf{f} = \sum_{m=1}^M \langle \mathbf{f}, \mathbf{e}_m \rangle \mathbf{e}_m$ for all $\mathbf{f} \in L_2(\mathcal{G})$, where $\langle \cdot, \cdot \rangle$ is the inner product and we denote $[M] := \{1, \dots, M\}$. We denote the i -th column vector and row vector of a matrix M , by $M_{:i}$ and $M_{i:}$ respectively.

For $K \geq 2$, we call a sequence $\mathcal{P}_K := \{\mathcal{V}_j : j = 1, \dots, K\}$ of sets as a *K-hierarchical clustering* of \mathcal{V} if each $\mathcal{V}_j := \{s_\Lambda \subset \mathcal{V} : \dim(\Lambda) = j\}$ is a partition of \mathcal{V} , i.e., $\mathcal{V} = \bigcup_\Lambda s_\Lambda$, and \mathcal{V}_j is a refinement of \mathcal{V}_{j-1} , where we use the index vector $\Lambda = (\lambda_1, \dots, \lambda_j) \in \mathbb{N}^j$ to encode position, level j , and parent-children relationship, of the clusters s_Λ . Figures 1 and 2 (top-right) give two examples on illustrating our notations. Here $\dim(\Lambda)$ denotes the length of the index vector. If $s_\Lambda \in \mathcal{V}_j$ is a parent, then the index vectors of its children are appended with an integer, i.e. (Λ, i) and thus the child is denoted by $s_{(\Lambda, i)} \in \mathcal{V}_{j+1}$. Then we have the parent-children relationship $s_{(\Lambda, i)} \subset s_\Lambda$. We denote the number of children of s_Λ by L_Λ . Unless specified, we consider K -hierarchical clustering \mathcal{P}_K with $\mathcal{V}_K = \{\{1\}, \dots, \{n\}\}$ and $\mathcal{V}_1 = \{[n]\}$ being a singleton, i.e., \mathcal{P}_K is a *tree*.

3.2 Main Construction

In classical wavelet/framelet theory, an important concept is the multiresolution analysis (MRA). One of the most important ideas is to find a sequence of subspaces $\{V_j\} \subset L_2(\mathbb{R})$ such that $V_j \subset V_{j+1}$ and $\bigcup_{j \in \mathbb{Z}} V_j = L_2(\mathbb{R})$. If there exists $\phi(t) \in V_0$ such that $\{\phi(t-b)\}_{b \in \mathbb{Z}}$ is an orthonormal basis of V_0 and $f(t) \in V_j$ if and only if $f(2t) \in V_{j+1}$, then we can find a mother wavelet $\psi(t)$ such that $\{2^{j/2} \psi(2^j t - b)\}_{j, b \in \mathbb{Z}}$ forms an orthonormal basis for $L_2(\mathbb{R})$. However, the translation and dilation operators are not naturally defined for graph signals. A natural way to define translations and dilations is to employ hierarchical partitions, see [29, 17]. Below, we provide general conditions in Theorem 3.1 for constructing Haar graph framelets based on a K -hierarchical clustering.

Given \mathcal{P}_K , we define the unit scaling vectors ϕ_Λ (similar to scaling functions for V_j on a MRA) iteratively from $\dim(\Lambda) = K$ to $\dim(\Lambda) = 1$. When $\dim(\Lambda) = K$, each cluster (node) s_Λ contains only one vertex in graph \mathcal{G} (see top-right of Figures 1 and 2), thus we define $\phi_\Lambda = \mathbf{I}_{:i}$, where $i \in s_\Lambda \subset \mathcal{V}$ and $\mathbf{I}_{:i}$ is the i -th column of the identity matrix $\mathbf{I} \in \mathbb{R}^{n \times n}$. When $\dim(\Lambda) < K$, we define

$$\phi_\Lambda := \sum_{\ell \in [L_\Lambda]} p_{(\Lambda, \ell)} \phi_{(\Lambda, \ell)}, \quad (1)$$

where $\mathbf{p}_\Lambda = [p_{(\Lambda, 1)}, \dots, p_{(\Lambda, L_\Lambda)}]^\top \in \mathbb{R}^{L_\Lambda}$ and $\|\mathbf{p}_\Lambda\| = 1$. Obviously, ϕ_Λ is with support $\text{supp} \phi_\Lambda = s_\Lambda$ and $\|\phi_\Lambda\| = 1$. For framelet vectors on the graph, we define $\psi_{(\Lambda, m)}$, $m \in [M_\Lambda]$ for some $M_\Lambda \in \mathbb{N}$ by

$$\psi_{(\Lambda, m)} := \sum_{\ell \in [L_\Lambda]} (\mathbf{B}_\Lambda)_{m, \ell} \phi_{(\Lambda, \ell)}, \quad (2)$$

from some matrix $\mathbf{B}_\Lambda \in \mathbb{R}^{M_\Lambda \times L_\Lambda}$. Theorem 3.1 characterizes when ϕ_Λ and $\psi_{(\Lambda, m)}$ form a tight frame of $L_2(\mathcal{G})$.

Theorem 3.1 (General characterization). *Let \mathcal{P}_K be a K -hierarchical clustering on a graph \mathcal{G} . Then the matrices \mathbf{B}_Λ and vectors \mathbf{p}_Λ satisfy $\mathbf{B}_\Lambda \mathbf{B}_\Lambda^\top \mathbf{B}_\Lambda = \mathbf{B}_\Lambda$, $\mathbf{B}_\Lambda \mathbf{p}_\Lambda = \mathbf{0}$, and $\text{Rank}(\mathbf{B}_\Lambda) = L_\Lambda - 1$ for all Λ with $\dim(\Lambda) = j_0, \dots, K$ if and only if for any $j_0 \in [K]$, the collection $\mathcal{F}_{j_0}(\mathcal{P}_K) := \{\phi_\Lambda : \dim(\Lambda) = j_0\} \cup \{\psi_\Lambda : \dim(\Lambda) = j\}_{j=j_0+1}^K$ defined by Equations (1) and (2) is a tight frame of $L_2(\mathcal{G})$.*

The proof of Theorem 3.1 is similar to [17] but steps further to a sufficient and necessary condition for all framelets that have the form 1 and 2. When we use graph Haar framelets to extract frequency features of graph signals, general graph wavelets/framelets (1 and 2) can be viewed as multi-scale representation systems in which the notion of ‘scale’ is different from the usual k -hop neighborhood in graphs and serve as an alternative to capture long-range information.

Besides, the given \mathcal{P}_K in the proposed construction is not specified. The advantage of the generality of this definition is that there is no constraint on how the \mathcal{P}_K is generated: one can use solely the edges or combine the edges and node features to generate \mathcal{P}_K , etc. Thus this provides great potential in theories and applications. As will be shown in experiments, clustering graph nodes based only on adjacency matrices is capable of providing nice graph framelets that help improve learning abilities of neural networks on node classification tasks.

The following example shows a close relationship between our framelet systems and traditional graph Haar basis.

Example 1 (Path graph and Haar basis). Given a path graph \mathcal{G}_1 with 8 nodes $\mathcal{V} = \{1, 2, \dots, 8\}$. If we choose hierarchical clustering $\mathcal{P}_4 = \{\mathcal{V}_1, \mathcal{V}_2, \mathcal{V}_3, \mathcal{V}_4\}$ with $\mathcal{V}_1 = \{s_{(1)}\}$, $\mathcal{V}_2 = \{s_{(1,1)}, s_{(1,2)}\}$, $\mathcal{V}_3 = \{s_{(1,1,1)}, s_{(1,1,2)}, s_{(1,2,1)}, s_{(1,2,2)}\}$, $\mathcal{V}_4 = \{s_{(1,1,1,1)}, s_{(1,1,1,2)}, s_{(1,1,2,1)}, s_{(1,1,2,2)}, s_{(1,2,1,1)}, s_{(1,2,1,2)}, s_{(1,2,2,1)}, s_{(1,2,2,2)}\}$, and $\mathbf{p}_\Lambda = [\frac{1}{\sqrt{2}}, \frac{1}{\sqrt{2}}]^\top$ and $\mathbf{B}_\Lambda = [\frac{1}{\sqrt{2}}, -\frac{1}{\sqrt{2}}]$ for all Λ (note that each parent has two exactly children $L_\Lambda = 2$), then the graph framelet system $\mathcal{F}_{j_0}(\mathcal{P}_K)$ with $K = 4$ as in Theorem 3.1 is a Haar basis for any $j_0 \in [K]$. See Figure 1 for illustration.

Since conditions in Theorem 3.1 is too general for use, next we want to investigate the properties that is helpful for constructing the proposed framelets. Notice that the role of elements in \mathbf{p}_Λ in 1 is to give weights to each cluster $s_{(\Lambda, \ell)}$. Hence, it is natural to claim that each children cluster is of equal importance, which means that the vector \mathbf{p}_Λ is a constant vector. Under this equal importance hypothesis, we give the following proposition that characterize the structure of matrices in Theorem 3.1.

Proposition 3.2. *Let vector $\mathbf{w} \in \mathbb{R}^L$ satisfies $\mathbf{w}^\top \mathbf{1} = 0$ and $\{\mathbf{P}_m\}_{m=1}^M \subset \mathbb{R}^{L \times L}$ be a set of permutation matrix. Define $\mathbf{B} := [\mathbf{P}_1 \mathbf{w}, \dots, \mathbf{P}_M \mathbf{w}]^\top \in \mathbb{R}^{M \times L}$. We assume that $\text{Rank}(\mathbf{B}) = L - 1$. Then the quantities $\sum_{m: |(\mathbf{P}_m \mathbf{w})_s| = a} |(\mathbf{P}_m \mathbf{w})_s| = d(a)$ for any s and $\sum_{m: (\mathbf{P}_m \mathbf{w})_s = a} (\mathbf{P}_m \mathbf{w})_t = b(a)$ for any $t > s$, where $a \in \{\mathbf{w}_i\} - \{0\}$ and $d(a), b(a) \in \mathbb{R}$ only depends on a if and only if there exists a constant c such that $\mathbf{B} \mathbf{B}^\top \mathbf{B} = c \mathbf{B}$.*

An intuitive understanding of Proposition 3.2 is that to obtain matrices \mathbf{B} we can permute the elements in \mathbf{w} such that each elements appears at each position with equal chance and then collect them in a single matrix. Combining Proposition 3.2 with 1 and 2, we have a theoretical guarantee (Corollary 3.3) of the perfect reconstruction.

Corollary 3.3. *Let c be a constant. Denote \mathbf{B} be defined in Proposition 3.2 which satisfies $\mathbf{B} \mathbf{B}^\top \mathbf{B} = c \mathbf{B}$. Let $\mathbf{P} = [\frac{1}{\sqrt{L}} \mathbf{1}, \frac{1}{\sqrt{c}} \mathbf{B}^\top]$. Then $\mathbf{P} \mathbf{P}^\top = \mathbf{I}$*

Theorem 3.1 gives a general framework to construct Haar-type framelet systems on graphs. In the following result, we introduce a binary Haar graph framelet system by a careful design of the matrices \mathbf{B}_Λ and \mathbf{p}_Λ . The word *binary* here is chosen since each nonzero coefficients of high frequency framelets 2 only takes from $\{1, -1\}$ (without normalization). We show that such graph framelet systems $\mathcal{F}_{j_0}(\mathcal{P}_K)$ have many desirable properties including permutation equivariance.

For each pair (ℓ_1, ℓ_2) with $1 \leq \ell_1 < \ell_2 \leq L_\Lambda$, define a vector \mathbf{w}_Λ^m of size $L_\Lambda \times 1$ by

$$(\mathbf{w}_\Lambda^m)_\tau = \begin{cases} \frac{1}{\sqrt{L_\Lambda}} & \tau = \ell_1; \\ \frac{-1}{\sqrt{L_\Lambda}} & \tau = \ell_2; \\ 0 & \text{otherwise,} \end{cases} \quad (3)$$

where $m := m(\ell_1, \ell_2, L_\Lambda) := \frac{(2L_\Lambda - \ell_1)(\ell_1 - 1)}{2} + \ell_2 - \ell_1$ is ranging from 1 to $M_\Lambda := \frac{L_\Lambda(L_\Lambda - 1)}{2}$ for all possible pairs (ℓ_1, ℓ_2) with $1 \leq \ell_1 < \ell_2 \leq L_\Lambda$. Note that \mathbf{w}_Λ^m has only two non-zero entries locating at the ℓ_1 -th and ℓ_2 -the columns. Such a \mathbf{w}_Λ^m will be used as the m -th row of the matrix \mathbf{B}_Λ .

Corollary 3.4 (Binary Haar graph framelets). *Let \mathcal{P}_K be a K -hierarchical clustering on a graph \mathcal{G} . Let $\mathbf{p}_\Lambda = \frac{1}{\sqrt{L_\Lambda}} \mathbf{1}$ be a vector of size $L_\Lambda \times 1$ and $\mathbf{B}_\Lambda := [\mathbf{w}_\Lambda^1, \dots, \mathbf{w}_\Lambda^{M_\Lambda}]^\top$ with \mathbf{w}_Λ^m being given as in Equation (3). Define $\mathcal{F}_{j_0}(\mathcal{P}_K)$ as in Theorem 3.1. Then $\mathcal{F}_{j_0}(\mathcal{P}_K)$ is a tight frame for $L_2(\mathcal{G})$ for any $j_0 \in [K]$.*

Example 2. Given a graph \mathcal{G}_2 with 7 nodes $\mathcal{V} = \{1, 2, \dots, 7\}$. We choose hierarchical clustering $\mathcal{P}_3 = \{\mathcal{V}_1, \mathcal{V}_2, \mathcal{V}_3\}$ with $\mathcal{V}_1 = \{s_{(1)}\}$, $\mathcal{V}_2 = \{s_{(1,1)}, s_{(1,2)}\}$, $\mathcal{V}_3 = \{s_{(1,1,1)}, s_{(1,2,1)}, s_{(1,2,2)}\}$, and \mathbf{p}_Λ and \mathbf{B}_Λ described as in Corollary 3.4. Note that $L_{(1)} = 2$, $L_{(1,1)} = 3$ and $L_{(1,2)} = 4$. The system $\mathcal{F}_{j_0}(\mathcal{P}_K)$ with $K = 3$ in Theorem 3.1 is a tight frame for any $j_0 \in [K]$. Figure 2 shows that our framelet is well-localized with multi-scale information.

Remark 3.5. In fact, the framelets obtained in Examples 1 and 2 are all binary Haar graph framelets (See Figures 1 and 2 for illustration). The matrix \mathbf{B}_Λ is formed by permuting 1, -1 of the vector $[1, -1, 0, \dots, 0]$ to all possible positions. More details of Examples 1 and 2 for Corollary 3.4 can be found in Appendix C. We next focus on the sparsity, efficiency, and permutation equivariance of the binary Haar graph framelets constructed in Corollary 3.4.

3.3 Fast Decomposition and Reconstruction Algorithms

Given a K -hierarchical clustering \mathcal{P}_K , we consider graph Haar framelet transform between V_{j+1} and $V_j \oplus W_j$. Define $x_{(\Lambda, \ell)} := \langle \mathbf{f}, \phi_{(\Lambda, \ell)} \rangle$ and $y_{(\Lambda, m)} := \langle \mathbf{f}, \psi_{(\Lambda, m)} \rangle$ for a given graph signal \mathbf{f} . The transform algorithm is to evaluate $x_{(\Lambda, \ell)}$ and $y_{(\Lambda, m)}$ effectively. Let $\mathbf{C}_\Lambda \in \mathbb{R}^{L_\Lambda \times (1+M_\Lambda)}$ be a matrix satisfying $\mathbf{C}_\Lambda \begin{pmatrix} \mathbf{p}_\Lambda^\top \\ \mathbf{B}_\Lambda \end{pmatrix} = \mathbf{I} \in \mathbb{R}^{L_\Lambda \times L_\Lambda}$. Then [17] and Equations (1) and (2) imply that

$$\begin{bmatrix} \phi_\Lambda^\top \\ \psi_{(\Lambda, 1)}^\top \\ \vdots \\ \psi_{(\Lambda, M_\Lambda)}^\top \end{bmatrix} := \begin{pmatrix} \mathbf{p}_\Lambda^\top \\ \mathbf{B}_\Lambda \end{pmatrix} \begin{bmatrix} \phi_{(\Lambda, 1)}^\top \\ \vdots \\ \phi_{(\Lambda, L_\Lambda)}^\top \end{bmatrix}, \quad \begin{bmatrix} \phi_{(\Lambda, 1)}^\top \\ \vdots \\ \phi_{(\Lambda, L_\Lambda)}^\top \end{bmatrix} := \mathbf{C}_\Lambda \begin{bmatrix} \phi_\Lambda^\top \\ \psi_{(\Lambda, 1)}^\top \\ \vdots \\ \psi_{(\Lambda, M_\Lambda)}^\top \end{bmatrix}. \quad (4)$$

For the decomposition algorithm, we are give a signal $\mathbf{f} \in V_{j+1}$, which means that

$$\mathbf{f} = \sum_{\dim(\Lambda)=j} \sum_{\ell \in [L_\Lambda]} x_{(\Lambda, \ell)} \phi_{(\Lambda, \ell)}.$$

By Equation (4), we have

$$\begin{aligned}
\mathbf{f} &= \sum_{\dim(\Lambda)=j} \sum_{\ell \in [L_\Lambda]} x_{(\Lambda, \ell)} \phi_{(\Lambda, \ell)} \\
&= \sum_{\dim(\Lambda)=j} \sum_{\ell \in [L_\Lambda]} x_{(\Lambda, \ell)} \left((C_\Lambda)_{\ell, 1} \phi_\Lambda + \sum_{m \in [M_\Lambda]} (C_\Lambda)_{\ell, m+1} \psi_{(\Lambda, m)} \right) \\
&= \sum_{\dim(\Lambda)=j} \phi_\Lambda \sum_{\ell \in [L_\Lambda]} x_{(\Lambda, \ell)} (C_\Lambda)_{\ell, 1} + \sum_{\dim(\Lambda)=j} \sum_{m \in [M_\Lambda]} \psi_{(\Lambda, m)} \sum_{\ell \in [L_\Lambda]} x_{(\Lambda, \ell)} (C_\Lambda)_{\ell, m+1} \\
&= \sum_{\dim(\Lambda)=j} x_\Lambda \phi_\Lambda + \sum_{\dim(\Lambda)=j} \sum_{m \in [M_\Lambda]} y_{(\Lambda, m)} \psi_{(\Lambda, m)},
\end{aligned} \tag{5}$$

where we can represent decomposition of \mathbf{f} with respect to each Λ as

$$[x_\Lambda, y_{(\Lambda, 1)}, \dots, y_{(\Lambda, M_\Lambda)}] = [x_{(\Lambda, 1)}, x_{(\Lambda, 2)}, \dots, x_{(\Lambda, L_\Lambda)}] C_\Lambda. \tag{6}$$

Conversely, if we have $\mathbf{f} \in V_j \oplus W_j$, which means that

$$\mathbf{f} = \sum_{\dim(\Lambda)=j} x_\Lambda \phi_\Lambda + \sum_{\dim(\Lambda)=j} \sum_{m \in [M_\Lambda]} y_{(\Lambda, m)} \psi_{(\Lambda, m)},$$

then, by Equation (4), for the reconstruction from $V_j \oplus W_j$ to V_{j+1} , we have

$$\begin{aligned}
\mathbf{f} &= \sum_{\dim(\Lambda)=j} x_\Lambda \phi_\Lambda + \sum_{\dim(\Lambda)=j} \sum_{m \in [M_\Lambda]} y_{(\Lambda, m)} \psi_{(\Lambda, m)} \\
&= \sum_{\dim(\Lambda)=j} \sum_{\ell \in [L_\Lambda]} (r_\Lambda)_\ell \phi_{(\Lambda, \ell)} \\
&= \sum_{\dim(\Lambda)=j} \sum_{\ell \in [L_\Lambda]} x_{(\Lambda, \ell)} \phi_{(\Lambda, \ell)},
\end{aligned} \tag{7}$$

where

$$r_\Lambda = x_\Lambda p_\Lambda^\top + y_\Lambda^\top B_\Lambda, \text{ with } y_\Lambda = [y_{(\Lambda, 1)}, \dots, y_{(\Lambda, M_\Lambda)}]^\top, \tag{8}$$

and $x_{(\Lambda, \ell)} := (r_\Lambda)_\ell$.

Algorithm 1 Fast framelet decomposition

Input: $\mathcal{P}_K, \{x_\Lambda : \dim(\Lambda) = j_0\}, \{C_\Lambda\}, j_1$
 initialize $\hat{\mathbf{f}} = \emptyset$.
for $j = j_0 - 1$ **to** j_1 **do**
for $\Lambda \in \{\Lambda : \dim(\Lambda) = j\}$ **do**
 $[x_\Lambda, y_{(\Lambda, 1)}, \dots, y_{(\Lambda, M_\Lambda)}] \leftarrow [x_{(\Lambda, 1)}, x_{(\Lambda, 2)}, \dots, x_{(\Lambda, L_\Lambda)}] C_\Lambda$
 update $\hat{\mathbf{f}} \leftarrow \hat{\mathbf{f}} \cup \{x_\Lambda, y_{(\Lambda, m)}, m = 1, \dots, M_\Lambda\}$

Output: $\mathcal{F}_{j_0}(\mathcal{P}_K)$

Hence, by using Equation (6) iteratively from V_K , given a framelet system $\mathcal{F}_{j_0}(\mathcal{P}_K)$ and a graph signal \mathbf{f} , we get the coefficient vector $\hat{\mathbf{f}}$ consisting of coefficients from

$$\mathbf{f} \mapsto \{x_\Lambda : \dim(\Lambda) = j_0\} \cup \{y_\Lambda : \dim(\Lambda) = j\}_{j=j_0+1}^{K-1} \tag{9}$$

with respect to $V_{j_0} \oplus W_{j_0} \oplus \dots \oplus W_{K-1}$. In the reconstruction process, we iteratively obtain the representation of \mathbf{f} in V_K from coefficient vector $\hat{\mathbf{f}}$:

$$\{x_\Lambda : \dim(\Lambda) = j_0\} \cup \{y_\Lambda : \dim(\Lambda) = j\}_{j=j_0+1}^{K-1} \mapsto \mathbf{f} \tag{10}$$

with respect to $V_{j_0} \oplus W_{j_0} \oplus \dots \oplus W_{K-1}$.

From the above discussion, we observe that decomposition and reconstruction algorithms do not need to form the full framelet system explicitly, but p_Λ, B_Λ and C_Λ . This enhances the efficiency of the graph neural networks.

Theorem 3.6. *Under the same assumption as in Corollary 3.4. The decomposition algorithm to obtain the framelet coefficient vector $\hat{\mathbf{f}}$ from \mathbf{f} and the reconstruction algorithm to obtain the graph signal \mathbf{f} from $\hat{\mathbf{f}}$, as described in Equations (9) and (10), are both with a computational complexity of order $O(nh)$.*

Algorithm 2 Fast framelet reconstruction

Input: \mathcal{P}_K , $\{x_\Lambda : \dim(\Lambda) = j_0\} \cup \{y_{(\Lambda, m)} : \dim(\Lambda) = j_0, m \in [M_\Lambda]\}$, $\{\mathbf{p}_\Lambda, \mathbf{C}_\Lambda\}$, j_1
 initialize $\mathbf{f} = \emptyset$
for $j = j_0 + 1$ **to** j_1 **do**
 for $\Lambda \in \{\Lambda : \dim(\Lambda) = j\}$ **do**
 $\mathbf{r}_\Lambda = x_\Lambda \mathbf{p}_\Lambda^\top + y_\Lambda^\top \mathbf{B}_\Lambda$
 for $\ell = 1$ **to** L_Λ **do**
 $x_{(\Lambda, \ell)} \leftarrow (\mathbf{r}_\Lambda)_\ell$
 update $\mathbf{f} \leftarrow \mathbf{f} \cup \{x_{(\Lambda, \ell)}\}_{\ell \in [L_\Lambda]}$
Output: \mathbf{f}

3.4 Sparsity

Notice that if each row of matrices \mathbf{B}_Λ is sparse, then the produced $\psi_{(\Lambda, m)}$ is also sparse. For the binary Haar graph framelets, each row of \mathbf{B}_Λ only contains two nonzero values. Let $L_j := \max_{\dim(\Lambda)=j} L_\Lambda$, then it is easy to see that the number $\|\psi_{(\Lambda, m)}\|_0$ of non-zero entries of $\psi_{(\Lambda, m)}$ satisfies $\|\psi_{(\Lambda, m)}\|_0 \leq 2L_{j+1}$, for all $\dim(\Lambda) = j$. When the hierarchical clustering is balanced and $\dim(\Lambda)$ is large, high-level framelets $\psi_{(\Lambda, m)}$ are well-localized and thus sparse.

Besides the sparsity of the framelets, we also want to know when the framelet coefficients of a signal are sparse. Different coefficients represent different scales. The pattern of framelet coefficients of signals is widely believed a useful tool for classification tasks. In node classification, piecewise constant signals are of great importance, e.g., in one-hot label encoding [2]. Hence, it is valuable to study the framelet coefficients of the piecewise constant signals. Let $\mathcal{F}_{j_0}(\mathcal{P}_K) := \{\phi_\Lambda, \dim(\Lambda) = j_0\} \cup \{\psi_\Lambda, \dim(\Lambda) = j\}_{j=j_0+1}^K =: \{\mathbf{u}_i\}_{i=1}^{M_G}$ be a binary Haar graph framelet system with M_G elements and define $\hat{\mathbf{f}} \in \mathbb{R}^{M_G}$ to be the *framelet coefficient vector* with elements $(\hat{\mathbf{f}})_i = \langle \mathbf{f}, \mathbf{u}_i \rangle$ for a signal \mathbf{f} . That is, denote $\mathbf{F} = [\mathbf{u}_1, \dots, \mathbf{u}_{M_G}]$. Then, $\hat{\mathbf{f}} = \mathbf{F}^\top \mathbf{f}$. We have the following result regarding the sparsity of $\hat{\mathbf{f}}$.

Theorem 3.7 (Binary Haar graph framelet transform preserving sparsity). *Let $\mathcal{F}_{j_0}(\mathcal{P}_K)$ be a binary Haar graph framelet system defined as in Corollary 3.4. Suppose that the signal $\mathbf{f} \in \mathbb{R}^n$ and $\max_{\dim(\Lambda)>0} L_\Lambda \leq h$. Then the framelet coefficient vector $\hat{\mathbf{f}}$ satisfies $\|\hat{\mathbf{f}}\|_0 \leq (K-1)(h-1)\|\mathbf{f}\|_0$.*

Remark 3.8. If for all Λ , we have $L_\Lambda = h$ for some integer $h \geq 2$, then $K = O(\log_h n)$ and hence $\|\hat{\mathbf{f}}\|_0 = \|\mathbf{f}\|_0 \cdot O(h \log_h n)$, which shows that our binary Haar graph transform preserves sparsity for sparse signals. In fact, the total number M_G of elements in $\mathcal{F}_{j_0}(\mathcal{P}_K)$ in this case is of order $O(nh)$. When $\|\mathbf{f}\|_0 \ll n$, we see that $\|\hat{\mathbf{f}}\|_0 \ll O(nh) = M_G$. Theorem 3.7 can be extended to other type of matrices \mathbf{B}_Λ that is row-wise sparse.

3.5 Efficiency

Graph Fourier basis based on graph Laplacian is of great importance in graph neural networks. However, the computational complexity and space complexity of generating graph Fourier basis could be as large as $O(n^3)$ and $O(n^2)$, respectively. Hence, these reasons prevent it from being more flexible in practice. On the other hand, when using our binary Haar graph framelets, we have an efficient way to compute our framelets as well as the framelet coefficient vector via sparse computation. For the rest of this paper, when we discuss computational complexity, we assume that all matrix/vector operations are sparse operations.

Theorem 3.9. *Let $h > 1$ be a positive integer. Assume that the K -hierarchical clustering \mathcal{P}_K satisfies $n = O(h^{K-1})$ with $h := \max_{\dim(\Lambda)>0} L_\Lambda$. For $j_0 \in [K]$, let $\mathcal{F}_{j_0}(\mathcal{P}_K) =: \{\mathbf{u}_m\}_{m=1}^{M_G}$ be the binary Haar graph framelet system as given in Corollary 3.4 and $\mathbf{F} = [\mathbf{u}_1, \dots, \mathbf{u}_{M_G}]$ be the framelet matrix with respect to $\mathcal{F}_{j_0}(\mathcal{P}_K)$. Then, for all $j_0 \in [K]$, the number M_G of elements in $\mathcal{F}_{j_0}(\mathcal{P}_K)$ is of order $O(nh)$, the computational complexity of generating all \mathbf{u}_m in \mathbf{F} is of order $O(nh \log_h n)$, and the total number $\text{nnz}(\mathbf{F})$ of nonzero entries in \mathbf{F} is of order $O(nh \log_h n)$.*

Remark 3.10. In practice, h is usually small (e.g., 2 or 4), and hence \mathbf{F} is a sparse matrix. Theorem 3.9 shows that our binary Haar graph framelet systems are efficient in processing datasets with large graphs. Moreover, the framelet coefficient vector $\hat{\mathbf{f}}$ can be computed with the computational complexity of order $O(nh \log_h n)$ as well.

3.6 Permutation Equivariance

The permutation equivariance is about **the consistency of a model's output**. Firstly, we would like to give a simple example to demonstrate its importance. Assume that we have a social network of 4 users A, B, C, and D. Each person

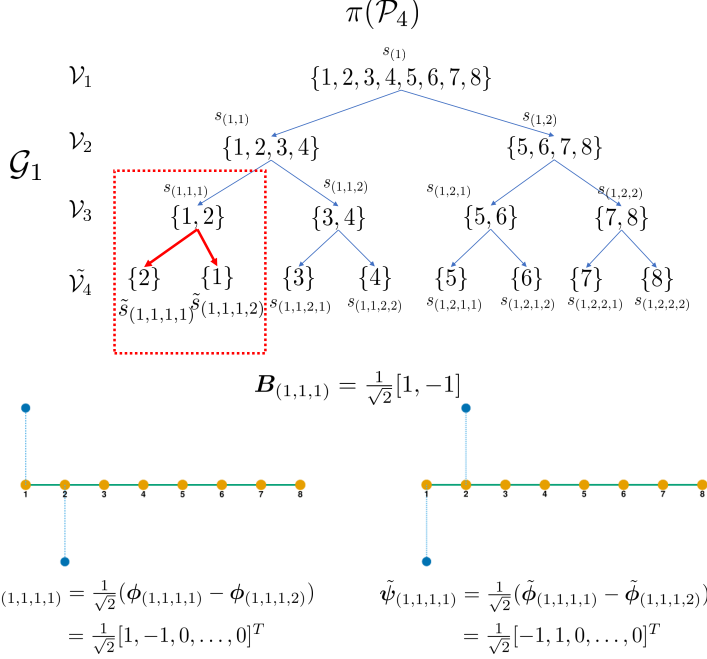


Figure 3: Partition permutation. The height of blue points represents the value of graph framelets, and they are above the graph if values are positive, and below otherwise. The red box indicates the permuted subtree. The bottom part shows a graph framelet and its variant after partition permutation.

has a user profile as features and friend relationships between users correspond to edges in 4-node graph. Our goal is to predict whether the users like a certain type of movie (labeled as 0 and 1). In practice, we would first number the users, e.g $A \rightarrow 1$, $B \rightarrow 2$, $C \rightarrow 3$, and $D \rightarrow 4$. Then we get an adjacency matrix $A \in \mathbb{R}^{4 \times 4}$. For a general GNN, we input the adjacency matrix and features and then receive the output. Let's say that the output vector is $(0, 1, 0, 1)$, which means B and D like it but A and C do not. If we number the users differently as $A \rightarrow 2$, $B \rightarrow 1$, $C \rightarrow 3$, $D \rightarrow 4$, then the output vector should correspondingly change to $(1, 0, 0, 1)$. In a word, permutation equivariance of a GNN ensures that if the nodes of a graph is permuted (i.e. reindexed, reordered), the outputs are also permuted correspondingly. Moreover, it can be seen that such a change of permutation does not affect the difference among nodes, just like that renumbering the users has nothing to do with the users' profile and friend relationships.

Fixed $\mathcal{G} = (\mathcal{V}, \mathcal{E})$ and \mathcal{P}_K , denote our construction of graph framelets in Theorem 3.1 by $\mathcal{A} : \mathcal{G} \times \mathcal{P}_K \rightarrow \mathcal{F}_{j_0}(\mathcal{P}_K)$. Let $\pi : \mathcal{V} \rightarrow \mathcal{V}$ be a reordering (relabelling, bijection) of $\mathcal{V} = \{1, 2, \dots, n\}$, i.e., π is w.r.t. a *node permutation* on $[n]$ with $\pi(\mathcal{V}) = \{\pi(1), \dots, \pi(n)\}$. We denote $\pi(\mathcal{G}) = (\pi(\mathcal{V}), \pi(\mathcal{E}))$ with $\pi(\mathcal{E}) := \{(\pi(i), \pi(j)) : (i, j) \in \mathcal{E}\}$. The corresponding signal \mathbf{f} on the graph \mathcal{G} is reordered to be $\pi(\mathbf{f})$ under the newly ordered graph $\pi(\mathcal{G})$. In other words, given a π , there exists a permutation matrix \mathbf{P}_π of size $n \times n$ such that $\pi(\mathbf{f}) = \mathbf{P}_\pi \mathbf{f}$. For each node permutation π , the construction \mathcal{A} is called (node) *permutation equivariant* if $\mathcal{A}(\pi(\mathcal{G}), \mathcal{P}_K) = \pi(\mathcal{A}(\mathcal{G}, \mathcal{P}_K))$, where $\pi(\mathbf{u}_m) = \mathbf{P}_\pi \mathbf{u}_m$ for $\mathbf{u}_m \in \mathcal{F}_{j_0}(\mathcal{P}_K)$.

Note that \mathcal{P}_K is a *tree* and that the children nodes in a parent-children subtree are ordered according to the last integer in the index vectors Λ . The order of nodes in such subtrees and the order of nodes in \mathcal{V} are separately defined. This means a reordering of nodes in \mathcal{V} does not affect the order in subtrees in \mathcal{P}_K and vice versa. On the other hand, the reordering of tree nodes Λ may result in different graph framelets. Figure 3 shows a simple example. Thus it is necessary to analyze the relationship of the graph framelets under such types of permutations. We say that π_p is a *partition permutation* on \mathcal{P}_K if the permutation is on the children of each tree node Λ only. For each partition permutation π_p , the construction \mathcal{A} is called *partition permutation equivariant* if $\mathcal{A}(\mathcal{G}, \pi_p(\mathcal{P}_K)) = \pi_p(\mathcal{A}(\mathcal{G}, \mathcal{P}_K))$, that is, there exists a permutation π^* on $[M_{\mathcal{G}}]$ associated with π_p such that for each $\mathbf{u}_m \in \mathcal{F}_{j_0}(\mathcal{P}_K)$, $\pi_p(\mathbf{u}_m) = c_m \mathbf{u}_{\pi^*(m)}$ for some $c_m \in \{-1, +1\}$. We have the following theorem regarding the permutation equivariance on both node and partition permutations. See Appendix A for more explanations.

Theorem 3.11. *Let $\mathcal{A} : \mathcal{G} \times \mathcal{P}_K \rightarrow \mathcal{F}_{j_0}(\mathcal{P}_K)$ be the construction of the binary Haar graph framelet systems in Corollary 3.4 for $j_0 \in [K]$. Then, the following three statements hold:*

- (i) For any node permutation π , we have $\mathcal{A}(\pi(\mathcal{G}), \mathcal{P}_K) = \pi(\mathcal{A}(\mathcal{G}, \mathcal{P}_K))$.
- (ii) For any partition permutation π_p , we have $\mathcal{A}(\mathcal{G}, \pi_p(\mathcal{P}_K)) = \pi_p(\mathcal{A}(\mathcal{G}, \mathcal{P}_K))$.
- (iii) For any node permutation π and partition permutation π_p , we have $\mathcal{A}(\pi(\mathcal{G}), \pi_p(\mathcal{P}_K)) = \pi_p(\pi(\mathcal{A}(\mathcal{G}, \mathcal{P}_K))) = \pi(\pi_p(\mathcal{A}(\mathcal{G}, \mathcal{P}_K)))$.

Theorem 3.11 shows that our binary framelet system $\mathcal{F}_{j_0}(\mathcal{P}_K)$ is permutation equivariant when reordering node or the tree indices. Hence the construction developed is robust for machine learning tasks.

This is a subtle property that most of the GNNs in the literature do not possess since they employ operations that only involve the adjacency matrix, the graph Laplacians, summation, and concatenation. Nonetheless, there are works ([22, 24]) that theoretically investigate the permutation equivariance of general and specific GNNs, which show a certain significance of this topic. On the contrary, graph wavelets/framelets, especially Haar-type graph wavelets/framelets are more complicatedly generated mathematical tools and the discussion of such property is missing in both the mathematical literature and the recent works of GNNs that apply graph wavelets/framelets. In some of the works of Haar-type graph wavelets/framelets, it is obvious that the permutation equivariance is violated if there are no further constraints. In contrast, our work is the first one to theoretically discuss and prove the permutation equivariance of Haar-type graph wavelets/framelets and the proposed GNN model Proposition 4.1.

4 GFNN Model

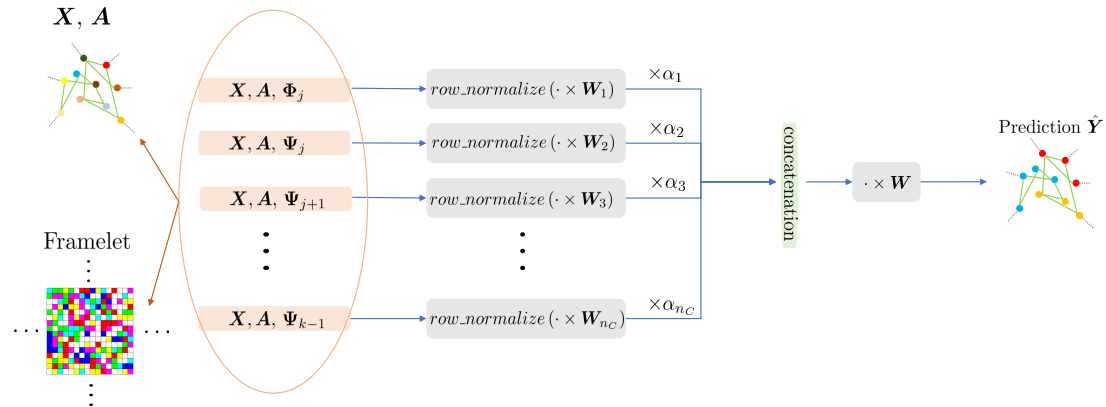


Figure 4: Neural network architecture.

We introduce the GFNN model that integrates our constructed binary Haar graph framelets, which we call **Permutation Equivariant Graph Framelet Augmented Network (PEGFAN)**, see Figure 4.

In a semi-supervised classification task, we assume that the first l nodes are labeled. Each node $i \in \mathcal{V}$ is associated with a feature vector $\mathbf{x}_i \in \mathbb{R}^{n_f}$ and a one-hot $\mathbf{y}_i \in \mathbb{R}^{n_c}$ indicating the ground truth of labels, where n_f and n_c are the numbers of features and classes. Stacking these vectors gives a feature matrix $\mathbf{X} \in \mathbb{R}^{n \times n_f}$ and a label matrix $\mathbf{Y} \in \mathbb{R}^{n \times n_c}$. Suppose there are n_C channels, associating a series of matrices $\mathbf{X}_1, \mathbf{X}_2, \dots, \mathbf{X}_{n_C}$ for each channel, and $\mathbf{X}_i \in \mathbb{R}^{n \times d_i}, 1 \leq i \leq n_C$. Our model is a two-layer network, which is defined as

$$\begin{aligned} \mathbf{H}_1 &= \big\|_{i=1}^{n_C} \alpha_i \cdot \text{row-nmz}(\mathbf{X}_i \mathbf{W}_i), \\ \hat{\mathbf{Y}} &= \text{softmax}(\text{ReLU}(\mathbf{H}_1) \mathbf{W}), \end{aligned}$$

where $\|$ denotes concatenation operation, α_i are trainable attention weights satisfying $\alpha_i \in (0, 1)$ and $\sum_i \alpha_i = 1$, $\text{row-nmz}(\mathbf{X}_i \mathbf{W}_i)$ is the row normalization operation, and $\mathbf{W}_i \in \mathbb{R}^{d_i \times n_h}$ and $\mathbf{W} \in \mathbb{R}^{n_C n_h \times n_c}$ are trainable parameters. As usual, we minimize the cross entropy of the labeled nodes using the first l columns of $\hat{\mathbf{Y}}$ and \mathbf{Y} .

Given the binary Haar graph framelet system $\mathcal{F}_{j_0}(\mathcal{P}_K)$, define Φ_j and Ψ_j to be matrices with rows to be $\{\phi_{\Lambda}\}_{\dim(\Lambda)=j}$ and $\{\psi_{(\Lambda, m)}\}_{\dim(\Lambda)=j, m \in [M_{\Lambda}]}$, respectively. We assume that the size of Φ_j and Ψ_j are $N_j \times n$ and $M_j \times n$, respectively. We denote $\mathbf{F}_0(\mathbf{M}) := \Phi_1^T \Phi_1 \mathbf{M}, \mathbf{F}_j(\mathbf{M}) := \Psi_j^T \Psi_j \mathbf{M}, 1 \leq j \leq K - 1$. For our GFNN model PEGFAN, we select

3 options for $\{\mathbf{X}_1, \dots, \mathbf{X}_{n_C}\}$ of feature matrices for graphs with homophily and heterophily, respectively. For homophilous graphs, we have 3 types:

- a) $n_C = 1 + K, \{\mathbf{X}, \mathbf{F}_0(\mathbf{X}), \mathbf{F}_1(\mathbf{X}), \dots, \mathbf{F}_{K-1}(\mathbf{X})\}.$
- b) $n_C = 1 + r + K, \{\mathbf{X}, \tilde{\mathbf{A}}\mathbf{X}, \tilde{\mathbf{A}}^2\mathbf{X}, \dots, \tilde{\mathbf{A}}^r\mathbf{X}, \mathbf{F}_0(\mathbf{X}), \mathbf{F}_1(\mathbf{X}), \dots, \mathbf{F}_{K-1}(\mathbf{X})\}.$
- c) $n_C = 1 + r + K, \{\mathbf{X}, \tilde{\mathbf{A}}\mathbf{X}, \tilde{\mathbf{A}}^2\mathbf{X}, \dots, \tilde{\mathbf{A}}^r\mathbf{X}, \mathbf{F}_0(\tilde{\mathbf{A}}\mathbf{X}), \mathbf{F}_1(\tilde{\mathbf{A}}\mathbf{X}), \dots, \mathbf{F}_{K-1}(\tilde{\mathbf{A}}\mathbf{X})\}.$

For heterophilous graphs, we have 3 types:

- a) $n_C = 1 + K, \{\mathbf{X}, \mathbf{F}_0(\mathbf{X}), \mathbf{F}_1(\mathbf{X}), \dots, \mathbf{F}_{K-1}(\mathbf{X})\}.$
- b) $n_C = 1 + r + K, \{\mathbf{X}, \mathbf{A}\mathbf{X}, \mathbf{A}^2\mathbf{X}, \dots, \mathbf{A}^r\mathbf{X}, \mathbf{F}_0(\mathbf{X}), \mathbf{F}_1(\mathbf{X}), \dots, \mathbf{F}_{K-1}(\mathbf{X})\}.$
- c) $n_C = 1 + r + K, \{\mathbf{X}, \mathbf{A}\mathbf{X}, \mathbf{A}^2\mathbf{X}, \dots, \mathbf{A}^r\mathbf{X}, \mathbf{F}_0(\mathbf{A}\mathbf{X}), \mathbf{F}_1(\mathbf{A}\mathbf{X}), \dots, \mathbf{F}_{K-1}(\mathbf{A}\mathbf{X})\}.$

With the permutation equivariance of our graph Haar framelet, now we can formally state the permutation equivariance of the model (see Appendix A for the proof).

Proposition 4.1. *Let $\mathcal{G} = (\mathcal{V}, \mathcal{E})$ be a graph with feature matrix \mathbf{X} , adjacency matrix \mathbf{A} , and a K -hierarchical partition \mathcal{P}_K . Let \mathbf{P} be a permutation matrix w.r.t. to a node permutation π on \mathcal{V} . If the permuted feature matrix $\mathbf{P}\mathbf{X}$, adjacency matrix $\mathbf{P}\mathbf{A}\mathbf{P}^\top$, and binary Haar graph framelet system $\pi(\mathcal{A}(\mathcal{G}, \mathcal{P}_K))$ are used in forming the type a), b) and c) channels for PEGFAN, then the new output $\hat{\mathbf{Y}}_{\mathbf{P}}$ differs from the original one by a permutation matrix, i.e. $\hat{\mathbf{Y}}_{\mathbf{P}} = \mathbf{P}\hat{\mathbf{Y}}$.*

Remark 4.2. In contrast to our PEGFAN, FSGNN [23] adopts the 2-layer network model with the following 3 options of input channels: 1) Homophily: $n_C = 1 + r, \{\mathbf{X}, \tilde{\mathbf{A}}\mathbf{X}, \tilde{\mathbf{A}}^2\mathbf{X}, \dots, \tilde{\mathbf{A}}^r\mathbf{X}\}$. 2) Heterophily: $n_C = 1 + r, \{\mathbf{X}, \mathbf{A}\mathbf{X}, \mathbf{A}^2\mathbf{X}, \dots, \mathbf{A}^r\mathbf{X}\}$. 3) All: $n_C = 1 + 2r, \{\mathbf{X}, \mathbf{A}\mathbf{X}, \tilde{\mathbf{A}}\mathbf{X}, \mathbf{A}^2\mathbf{X}, \tilde{\mathbf{A}}^2\mathbf{X}, \dots, \mathbf{A}^r\mathbf{X}, \tilde{\mathbf{A}}^r\mathbf{X}\}$.

As shown in Figure 4, our network model differs significantly from existing GNNs using graph wavelets/framelets in the sense that we fully utilize the multi-scale property of our Haar framelets as well as the powers of the adjacency matrix as **the multi-channel inputs**. In such a way, short- and long-range information of the graph is fully exploited for the training of the network model. On the contrary, neural architectures of other existing GNNs using graph wavelets/framelets are similar to classical spectral graph neural networks, which are essentially different from ours in exploiting multi-scale information. In the experiments, the claimed superiority is observed on synthetic datasets and graph node classification tasks.

5 Experiments

5.1 Synthetic Dataset

In [21], it has been theoretically shown that for a linear classifier, using $\mathbf{A}_{rw} := \mathbf{D}^{-1}\mathbf{A}$ to aggregate features has a lower probability to misclassify under the condition that the “neighborhood class distributions” are distinguishable. To elaborate, it assumes that for each node i of class $y_i = c$, the neighbors of i are sampled from a distribution \mathcal{D}_{y_i} , and the \mathcal{D}_c are different. For heterophilous graphs, it is possible to fit the aforementioned condition as long as for each node of some class, the connection pattern with nodes from each class is different from the patterns of nodes of a different class. In other words, using simple neighborhood aggregation such as $\mathbf{A}_{rw}\mathbf{X}$ in GNNs still has the chance to achieve good performance for heterophilous graphs and the experiments in [21] has empirically validated this statement.

Following their observation, we are interested in how the neighborhood distribution \mathcal{D}_c affects the performance of FSGNN and PEGFAN. We follow the way in [21] and generate 4-class heterophilous graphs with 3000 nodes, fixed Gaussian features, and different neighborhood class distributions. The proportion of training, validation, and test set was set to 48%, 32%, and 20%, respectively. We compare the performance of PEGFAN with FSGNN to demonstrate the ability of multi-scale extraction when our binary Haar graph framelet system is added. To emphasize the difference between graph framelets and K -hop aggregation, we **excluded** the feature matrix channel \mathbf{X} in the overall channels. A hyperparameter $\gamma \in [0, 1]$ indicates the tendency to sample edges from uniform neighborhood class distribution. Implementation details are the same as shown in the next subsection. Other details are in Appendix D.

Table 1 collects results that strictly follow the procedure defined in Appendix D. Table 2 contains results of replacing features sampled Gaussian distributions with closer means, which are more similar for different classes and more difficult to classify. Both tables still show that with addition of our Haar graph framelets, the model is able to perform better.

Table 1: Features sampled from $6(-0.75 + 0.5c)\xi$, where $\xi \sim N(0, 1)$, $c \in \{0, 1, 2, 3\}$.

γ	0	0.2	0.4	0.6	0.8	1
ours(Type b)	95.7	92.3	86	74.3	61	54
FSGNN(r=3)	91.7	82.3	74.2	61.5	51.8	46.8

Table 2: Features sampled from $(-0.75 + 0.5c)\xi$, where $\xi \sim N(0, 1)$, $c \in \{0, 1, 2, 3\}$.

γ	0	0.2	0.4	0.6	0.8	1
ours(Type b)	91.3	88.5	77.5	62.7	53.7	42
FSGNN(r=3)	91.8	80.8	70.7	64.5	50.5	44.2

5.2 Benchmark Datasets

Table 3: Dataset statistics, classification accuracy, and standard deviation. **Best** in bold, **second best** in blue.

	Cora	Citeseer	Pubmed	Texas	Wisconsin	Cornell	Actor	Chameleon	Squirrel
Node	2,708	3,327	19,717	183	251	183	7,600	2,277	5,201
$\ \mathbf{A}\ _0$	10,556	9,228	88,651	325	515	298	30,019	36,101	217,073
Feature	1,433	3,703	500	1,703	1,703	1,703	931	2,325	2,089
Density	$1.44 \cdot 10^{-3}$	$8.34 \cdot 10^{-4}$	$2.28 \cdot 10^{-4}$	$9.70 \cdot 10^{-3}$	$8.17 \cdot 10^{-3}$	$8.90 \cdot 10^{-3}$	$5.20 \cdot 10^{-4}$	$6.96 \cdot 10^{-3}$	$8.02 \cdot 10^{-3}$
Class	6	7	3	5	5	5	5	5	5
Type	Homophily	Homophily	Homophily	Heterophily	Heterophily	Heterophily	Heterophily	Heterophily	Heterophily
Mixhop	87.61 ± 0.85	76.26 ± 1.33	85.31 ± 0.61	77.84 ± 7.73	75.88 ± 4.90	73.51 ± 6.34	32.22 ± 2.34	60.50 ± 2.53	43.80 ± 1.48
GEOM-GCN	85.27	77.99	90.05	67.57	64.12	60.81	31.63	60.90	38.14
GCNII	88.01 ± 1.33	77.13 ± 1.38	90.30 ± 0.37	77.84 ± 5.64	81.57 ± 4.98	76.49 ± 4.37	-	62.48 ± 2.74	-
H2GCN-1	86.92 ± 1.37	77.07 ± 1.64	89.40 ± 0.34	84.86 ± 6.77	86.67 ± 4.69	82.16 ± 4.80	35.86 ± 1.03	57.11 ± 1.58	36.42 ± 1.89
WRGAT	88.20 ± 2.26	76.81 ± 1.89	88.52 ± 0.92	83.62 ± 5.50	86.98 ± 3.78	81.62 ± 3.90	36.53 ± 0.77	65.24 ± 0.87	48.85 ± 0.78
GPRGNN	88.49 ± 0.95	77.08 ± 1.63	88.99 ± 0.40	86.49 ± 4.83	85.88 ± 3.70	81.89 ± 6.17	36.04 ± 0.96	66.47 ± 2.47	49.03 ± 1.28
FSGNN(r=3)	86.92 ± 1.66	77.18 ± 1.27	89.71 ± 0.45	84.51 ± 4.71	87.84 ± 3.37	84.86 ± 4.56	35.26 ± 1.01	78.60 ± 0.71	73.93 ± 2.00
FSGNN(r=8)	88.15 ± 1.15	77.23 ± 1.41	89.67 ± 0.45	86.76 ± 3.72	87.65 ± 3.51	85.95 ± 5.10	35.22 ± 0.96	79.01 ± 1.23	73.78 ± 1.58
FSGNN(r=3,all)	87.59 ± 1.03	76.91 ± 1.60	89.68 ± 0.37	84.60 ± 5.41	86.67 ± 2.75	86.22 ± 6.78	35.51 ± 0.89	77.68 ± 1.10	73.79 ± 2.32
FSGNN(r=8,all)	87.53 ± 1.37	76.86 ± 1.49	89.73 ± 0.40	82.70 ± 5.01	85.88 ± 5.02	85.13 ± 7.57	35.28 ± 0.79	77.94 ± 1.17	74.04 ± 1.51
Ours($h = 4$, Type a)	79.48 ± 2.68	71.29 ± 2.01	88.46 ± 0.35	83.78 ± 5.54	86.08 ± 4.34	85.95 ± 5.51	34.96 ± 1.24	65.83 ± 2.05	51.98 ± 1.98
Ours($h = 4$, Type b)	87.12 ± 0.91	77.39 ± 1.28	89.62 ± 0.25	86.47 ± 5.54	86.67 ± 3.59	85.14 ± 5.57	35.07 ± 1.03	79.63 ± 1.23	73.89 ± 1.89
Ours($h = 4$, Type c)	87.36 ± 1.09	76.78 ± 1.51	89.55 ± 0.32	85.14 ± 4.05	87.65 ± 4.02	86.76 ± 5.33	35.41 ± 0.82	79.65 ± 1.33	74.58 ± 2.07
Ours($h = 8$, Type a)	83.16 ± 1.86	73.51 ± 1.67	88.85 ± 0.30	84.32 ± 3.78	86.67 ± 3.80	84.05 ± 6.10	35.15 ± 0.77	-	-
Ours($h = 8$, Type b)	87.22 ± 1.21	76.76 ± 1.40	89.73 ± 0.40	84.87 ± 5.70	85.69 ± 3.29	84.60 ± 5.41	35.34 ± 0.81	-	-
Ours($h = 8$, Type c)	87.16 ± 1.31	76.92 ± 1.57	89.56 ± 0.30	86.22 ± 3.30	86.67 ± 4.28	86.22 ± 4.75	35.48 ± 0.94	80.31 ± 1.10	75.06 ± 1.72

We conducted experiments on 9 datasets including 3 homophilous citation networks and 6 heterophilous datasets and followed the public data splits provided in [26]. We define the density of a graph as $\|\mathbf{A}\|_0/n^2$, which is the proportion between the number of non-zero terms in \mathbf{A} and the numbers of terms of \mathbf{A} . The statistics is summarized in the top rows of Table 3. To generate a series of partitions for each dataset, we applied `sknetwork.hierarchy.Ward` and `sknetwork.hierarchy.cut_balanced` from python package `scikit-network`^{*} to form intermediate clusters. Details are shown in Appendix E. As for the implementation of the neural network, we adopted the publicly released code of FSGNN^{*} for integrating the graph framelet projections as detailed in our PEGFAN model. We use the same optimizer, hidden layer size, etc., as those in FSGNN, and hence the details are omitted. We noticed that the outcome of FSGNN was a bit different from those reported in [23] when we tried to reproduce the results. Therefore we did a separate grid search for FSGNN and the results had slight changes. For our model, we set r of input channels to 3. Results of other models (Mixhop[1], GEOM-GCN[26], GCNII[3], H2GCN-1[36], WRGAT[27], GPRGNN[4]) are cited from [23] and the results of some of the top rows are omitted, which are not among the models with relatively superior performance. All of the results are collected in Table 3.

Table 4 summarizes the average, maximum, and minimum training time of our model and FSGNN on Chameleon and Squirrel over 108 sets of hyperparameters. Each training consists of 10 individual training on each data split. All experiments are conducted using an RTX 3090 graphics card.

5.3 Comments

For the synthetic dataset, it can be seen that the performance decreases with respect to γ (if $\gamma \rightarrow 1$ then, the graph is close to the case of being generated by uniform neighborhood class distribution). *Type b channels* input, in which graph

^{*}<https://scikit-network.readthedocs.io/>

^{*}<https://github.com/sunilkmaurya/FSGNN/>

framelets project the original feature matrix \mathbf{X} , show a large improvement compared with FSGNN. In some cases, the increment can reach over 10%. This evidently shows the effectiveness of multi-scale extractions via graph framelets when combined with adjacency matrix aggregations. There are also drawbacks, which can be seen from the results of *type a channels input* in ???. It shows that using graph framelets alone is not enough. Indeed, we chose a rather simple and unsupervised way to generate hierarchical clustering. This process altered the representation of the connectivity among nodes and caused a loss of information. Therefore, it is better to combine fine-scale information using 1 to 3-hop aggregation and coarse scale projection via graph framelets. It is also obvious that the neighborhood distributions affect our model performance given the theory in [21], in which the model accuracies decreased as the neighborhood distributions approached the same and indistinguishable uniform distribution.

As for the benchmark datasets, our model produces noticeable increases in accuracies on two relatively larger and denser heterophilous datasets *Chameleon* and *Squirrel*. Being heterophilous makes it necessary to gather multi-scale information, and denser graphs facilitate forming better series of partitions and thus better graph framelets. This is also consistent with the empirical results of the synthetic dataset since as shown in [21], the neighborhood distributions of *Chameleon* and *Squirrel* are distinguishable enough for different classes, while other heterophilous datasets either are small datasets that suffer from bias or do not fit such condition. For the homophilous datasets, their nature of being homophilous does not necessitate the need for further multi-scale information, and thus our method has a similar performance.

6 Conclusion

This paper proposes a novel and general method to construct Haar-type framelets on graphs that are permutation equivariant. It aims to serve as an alternative and supplement for multi-hop aggregations using powers of adjacency matrices. The results show that combining graph framelets and multi-hop aggregation increases the performance of node classification on heterophilous graphs in both synthetic and real-world data. Moreover, compared with using multi-hop aggregation alone, in the synthetic case our model shows significant increases against the deterioration of neighborhood distribution and results show consistency between the synthetic and benchmark datasets in terms of the patterns of neighborhood distribution. The overall results validate the capability of our graph framelets to extract multi-scale information under certain conditions and its superior performance. Finally, we would also like to mention that choosing a more sophisticated way to generate the hierarchical partitions has the potential to produce better graph framelets, which will be a future experimental direction to explore.

References

- [1] S. Abu-El-Haija, B. Perozzi, A. Kapoor, N. Alipourfard, K. Lerman, H. Harutyunyan, G. Ver Steeg, and A. Galstyan. Mixhop: Higher-order graph convolutional architectures via sparsified neighborhood mixing. In *international conference on machine learning*, pages 21–29. PMLR, 2019.
- [2] J. Brownlee. Why one-hot encode data in machine learning. *Machine Learning Mastery*, pages 1–46, 2017.
- [3] M. Chen, Z. Wei, Z. Huang, B. Ding, and Y. Li. Simple and deep graph convolutional networks. In *International Conference on Machine Learning*, pages 1725–1735. PMLR, 2020.
- [4] E. Chien, J. Peng, P. Li, and O. Milenkovic. Adaptive universal generalized pagerank graph neural network. In *ICLR*, 2021.
- [5] C. K. Chui, F. Filbir, and H. N. Mhaskar. Representation of functions on big data: graphs and trees. *Applied and Computational Harmonic Analysis*, 38(3):489–509, 2015.

Table 4: Training time.

Chameleion	average	maximum	minimum
FSGNN(r=3)	20.71s	64.68s	11.21s
FSGNN(r=8)	37.41s	90.7s	17.75s
Ours(Type c)	47.66s	125.25s	22.52s
Squirrel	average	maximum	minimum
FSGNN(r=3)	34.57s	83.24s	18.58s
FSGNN(r=8)	53.40s	141.24s	26.52s
Ours(Type c)	59.82s	198.77s	32.87s

- [6] C. K. Chui, H. Mhaskar, and X. Zhuang. Representation of functions on big data associated with directed graphs. *Applied and Computational Harmonic Analysis*, 44(1):165–188, 2018.
- [7] M. Crovella and E. Kolaczyk. Graph wavelets for spatial traffic analysis. In *IEEE INFOCOM 2003. Twenty-second Annual Joint Conference of the IEEE Computer and Communications Societies (IEEE Cat. No. 03CH37428)*, volume 3, pages 1848–1857. IEEE, 2003.
- [8] I. Daubechies. *Ten lectures on wavelets*. SIAM, 1992.
- [9] M. Defferrard, X. Bresson, and P. Vandergheynst. Convolutional neural networks on graphs with fast localized spectral filtering. *Advances in neural information processing systems*, 29, 2016.
- [10] B. Dong. Sparse representation on graphs by tight wavelet frames and applications. *Applied and Computational Harmonic Analysis*, 42(3):452–479, 2017.
- [11] M. Gavish, B. Nadler, and R. R. Coifman. Multiscale wavelets on trees, graphs and high dimensional data: Theory and applications to semi supervised learning. In *ICML*, 2010.
- [12] W. Hamilton, Z. Ying, and J. Leskovec. Inductive representation learning on large graphs. *Advances in neural information processing systems*, 30, 2017.
- [13] D. K. Hammond, P. Vandergheynst, and R. Gribonval. Wavelets on graphs via spectral graph theory. *Applied and Computational Harmonic Analysis*, 30(2):129–150, 2011.
- [14] B. Han. Framelets and wavelets. *Algorithms, Analysis, and Applications, Applied and Numerical Harmonic Analysis. Birkhäuser xxxiii Cham*, 2017.
- [15] B. Han, T. Li, and X. Zhuang. Directional compactly supported box spline tight framelets with simple geometric structure. *Applied Mathematics Letters*, 91:213–219, 2019.
- [16] T. N. Kipf and M. Welling. Semi-supervised classification with graph convolutional networks. In *5th International Conference on Learning Representations, ICLR 2017, Toulon, France, April 24-26, 2017, Conference Track Proceedings*. OpenReview.net, 2017.
- [17] J. Li, H. Feng, and X. Zhuang. Convolutional neural networks for spherical signal processing via area-regular spherical haar tight framelets. *IEEE Transactions on Neural Networks and Learning Systems*, 2022.
- [18] M. Li, Z. Ma, Y. G. Wang, and X. Zhuang. Fast haar transforms for graph neural networks. *Neural Networks*, 128:188–198, 2020.
- [19] Q. Li, Z. Han, and X.-M. Wu. Deeper insights into graph convolutional networks for semi-supervised learning. In *Thirty-Second AAAI conference on artificial intelligence*, 2018.
- [20] D. Lim, F. Hohne, X. Li, S. L. Huang, V. Gupta, O. Bhalerao, and S. N. Lim. Large scale learning on non-homophilous graphs: New benchmarks and strong simple methods. *Advances in Neural Information Processing Systems*, 34:20887–20902, 2021.
- [21] Y. Ma, X. Liu, N. Shah, and J. Tang. Is homophily a necessity for graph neural networks? In *International Conference on Learning Representations*, 2022.
- [22] H. Maron, H. Ben-Hamu, N. Shamir, and Y. Lipman. Invariant and equivariant graph networks. In *International Conference on Learning Representations*.
- [23] S. K. Maurya, X. Liu, and T. Murata. Simplifying approach to node classification in graph neural networks. *Journal of Computational Science*, 62:101695, 2022.
- [24] C. Morris, G. Rattan, S. Kiefer, and S. Ravanbakhsh. Speqnets: Sparsity-aware permutation-equivariant graph networks. In *International Conference on Machine Learning*, pages 16017–16042. PMLR, 2022.
- [25] H. Nt and T. Maehara. Revisiting graph neural networks: All we have is low-pass filters. *arXiv preprint arXiv:1905.09550*, 2019.
- [26] H. Pei, B. Wei, K. C. Chang, Y. Lei, and B. Yang. Geom-gcn: Geometric graph convolutional networks. In *8th International Conference on Learning Representations, ICLR 2020, Addis Ababa, Ethiopia, April 26-30, 2020*. OpenReview.net, 2020.
- [27] S. Suresh, V. Budde, J. Neville, P. Li, and J. Ma. Breaking the limit of graph neural networks by improving the assortativity of graphs with local mixing patterns. *Proceedings of the 27th ACM SIGKDD Conference on Knowledge Discovery & Data Mining*, 2021.
- [28] Y. G. Wang and X. Zhuang. Tight framelets and fast framelet filter bank transforms on manifolds. *Applied and Computational Harmonic Analysis*, 48(1):64–95, 2020.

- [29] Y. Xiao and X. Zhuang. Adaptive directional haar tight framelets on bounded domains for digraph signal representations. *Journal of Fourier Analysis and Applications*, 27(2):1–26, 2021.
- [30] K. Xu, C. Li, Y. Tian, T. Sonobe, K.-i. Kawarabayashi, and S. Jegelka. Representation learning on graphs with jumping knowledge networks. In *International conference on machine learning*, pages 5453–5462. PMLR, 2018.
- [31] R. Ying, R. He, K. Chen, P. Eksombatchai, W. L. Hamilton, and J. Leskovec. Graph convolutional neural networks for web-scale recommender systems. In *Proceedings of the 24th ACM SIGKDD international conference on knowledge discovery & data mining*, pages 974–983, 2018.
- [32] M. Zhang, Z. Cui, M. Neumann, and Y. Chen. An end-to-end deep learning architecture for graph classification. In *Proceedings of the AAAI conference on artificial intelligence*, volume 32, 2018.
- [33] X. Zheng, Y. Liu, S. Pan, M. Zhang, D. Jin, and P. S. Yu. Graph neural networks for graphs with heterophily: A survey. *arXiv preprint arXiv:2202.07082*, 2022.
- [34] X. Zheng, B. Zhou, Y. G. Wang, and X. Zhuang. Decimated framelet system on graphs and fast g-framelet transforms. *Journal of Machine Learning Research*, 23(18):1–68, 2022.
- [35] Y. Zhou, H. Zheng, X. Huang, S. Hao, D. Li, and J. Zhao. Graph neural networks: Taxonomy, advances, and trends. *ACM Trans. Intell. Syst. Technol.*, 13(1), jan 2022.
- [36] J. Zhu, Y. Yan, L. Zhao, M. Heimann, L. Akoglu, and D. Koutra. Beyond homophily in graph neural networks: Current limitations and effective designs. *Advances in Neural Information Processing Systems*, 33:7793–7804, 2020.

A Proofs of results in Section 3

Proof of Theorem 3.1. We denote $\Phi_j = \{\phi_\Lambda\}_{\dim(\Lambda)=j}$ and $\Psi_j = \{\psi_{(\Lambda,m)}\}_{\dim(\Lambda)=j, m \in [M_\Lambda]}$. Let $V_j := \text{span}\Phi_j$ and $W_j := \text{span}\Psi_j$. Note that supports of ϕ_Λ and $\phi_{\Lambda'}$ are disjoint. So are $\psi_{(\Lambda,m)}$ and $\psi_{(\Lambda',m')}$. Hence, by definition and $\|p_\Lambda\|_2 = 1$, we can see that Φ_j forms an orthonormal basis of V_j iteratively. Thus by Lemma 1 in [17], the conditions $B_\Lambda B_\Lambda^\top B_\Lambda = B_\Lambda$, $B_\Lambda p_\Lambda = 0$, and $\text{Rank}(B_\Lambda) = L_\Lambda - 1$ implies that $V_{j+1} = V_j \oplus W_j$ and $\{\phi_\Lambda\}_{\dim(\Lambda)=j} \cup \{\psi_{(\Lambda,m)}\}_{\dim(\Lambda)=j, m \in [M_\Lambda]}$ is a tight frame of V_{j+1} . Iteratively, for $j_0 < j$, we deduce that $V_{j_0} \oplus W_{j_0} \oplus \dots \oplus W_{j-1} = V_j$ and $\Phi_{j_0} \cup \Psi_{j_0} \cup \dots \cup \Psi_{j-1}$ is a tight frame for V_j . Now the conclusion of the theorem follows by letting $j = K$ and noting that $\mathcal{F}_{j_0}(\mathcal{P}_K) = \Phi_{j_0} \cup \Psi_{j_0} \cup \dots \cup \Psi_{K-1}$ as well as $V_K = L_2(\mathcal{G})$. In other words, by Lemma 1 in [17], for any $\mathbf{f} \in V_{j+1} = \text{span}\Phi_j$, we have

$$\mathbf{f} = \sum_{\mathbf{v} \in \Phi_{j+1}} \langle \mathbf{f}, \mathbf{v} \rangle \mathbf{v} = \sum_{\mathbf{v} \in \Phi_j} \langle \mathbf{f}, \mathbf{v} \rangle \mathbf{v} + \sum_{\mathbf{w} \in \Psi_j} \langle \mathbf{f}, \mathbf{w} \rangle \mathbf{w} = \mathbf{f}_j + \mathbf{g}_j,$$

where $\mathbf{f}_j := \sum_{\mathbf{v} \in \Phi_j} \langle \mathbf{f}, \mathbf{v} \rangle \mathbf{v}$ and $\mathbf{g}_j := \sum_{\mathbf{w} \in \Psi_j} \langle \mathbf{f}, \mathbf{w} \rangle \mathbf{w}$. Since $\Phi_{j-1} \cup \Psi_{j-1}$ forms a tight frame of V_j and $V_j \perp W_j$, we have

$$\begin{aligned} \mathbf{f} &= \mathbf{f}_j + \mathbf{g}_j \\ &= \sum_{\mathbf{v} \in \Phi_{j-1}} \langle \mathbf{f}_j, \mathbf{v} \rangle \mathbf{v} + \sum_{\mathbf{w} \in \Psi_{j-1}} \langle \mathbf{f}_j, \mathbf{w} \rangle \mathbf{w} + \mathbf{g}_j \\ &= \sum_{\mathbf{v} \in \Phi_{j-1}} \langle \mathbf{f}, \mathbf{v} \rangle \mathbf{v} + \sum_{\mathbf{w} \in \Psi_{j-1}} \langle \mathbf{f}, \mathbf{w} \rangle \mathbf{w} + \mathbf{g}_j \\ &= \mathbf{f}_{j-1} + \mathbf{g}_{j-1} + \mathbf{g}_j = \dots = \mathbf{f}_{j_0} + \mathbf{g}_{j_0} + \dots + \mathbf{g}_j. \end{aligned}$$

Thus we conclude that $\Phi_{j_0} \cup \Psi_{j_0} \cup \dots \cup \Psi_{j-1}$ is a tight frame of $V_j = V_{j_0} \oplus W_{j_0} \oplus \dots \oplus W_{j-1}$.

Conversely, if $\mathcal{F}_{j_0}(\mathcal{P}_k)$ is tight for any j_0 , then for any $\mathbf{f} \in L_2(\mathcal{G})$,

$$\begin{aligned} \mathbf{f} &= \sum_{\Lambda: \dim(\Lambda)=j_0} x_\Lambda \phi_\Lambda + \sum_{\Lambda: \dim(\Lambda) \geq j_0} \sum_{m \in [M_\Lambda]} y_{(\Lambda,m)} \psi_{(\Lambda,m)} \\ &= \sum_{\Lambda: \dim(\Lambda)=j_0+1} x_\Lambda \phi_\Lambda + \sum_{\Lambda: \dim(\Lambda) \geq j_0+1} \sum_{m \in [M_\Lambda]} y_{(\Lambda,m)} \psi_{(\Lambda,m)}, \end{aligned} \tag{11}$$

where $x_\Lambda := \langle \mathbf{f}, \phi_\Lambda \rangle$ and $y_\Lambda := \langle \mathbf{f}, \psi_\Lambda \rangle$. Then we obtain

$$\begin{aligned} &\sum_{\Lambda: \dim(\Lambda)=j_0+1} x_\Lambda \phi_\Lambda \\ &= \sum_{\Lambda: \dim(\Lambda)=j_0} x_\Lambda \phi_\Lambda + \sum_{\Lambda: \dim(\Lambda)=j_0} \sum_{m \in [M_\Lambda]} y_{(\Lambda,m)} \psi_{(\Lambda,m)}, \forall \mathbf{f} \in L_2(\mathcal{G}), \end{aligned} \tag{12}$$

Note that $\{\phi_\Lambda : \dim(\Lambda) = j_0 + 1\} = \{\phi_{(\Lambda,\ell)} : \dim(\Lambda) = j_0, \ell \in [L_\Lambda]\}$ forms an orthonormal system and $\psi_{(\Lambda,m)}$ is a linear combination of $\{\phi_{(\Lambda,\ell)} : \ell \in [L_\Lambda]\}$. Hence, by Equation (12), fixing a Λ , we have

$$\sum_{\ell \in [L_\Lambda]} x_{(\Lambda,\ell)} \phi_{(\Lambda,\ell)} = x_\Lambda \phi_\Lambda + \sum_{m \in [M_\Lambda]} y_{(\Lambda,m)} \psi_{(\Lambda,m)}.$$

As a result, the collection $\{\phi_\Lambda, \psi_{(\Lambda,1)}, \dots, \psi_{(\Lambda,M_\Lambda)}\}$ forms a tight frame of $\text{span}\{\phi_{(\Lambda,\ell)} : \dim(\Lambda) = j_0, \ell \in [L_\Lambda]\}$. The condition $\{\phi_\Lambda\} \perp \{\psi_{(\Lambda,m)}\}_{m=1}^{M_\Lambda}$, together with Lemma 1 in [17] implies the theorem. \square

Proof of Proposition 3.2. For simplicity, we denote $\{\mathbf{w}_i\} := \{\mathbf{w}_i\}_{i=1}^L$ as a set of all different values of elements of any given vector $\mathbf{w} \in \mathbb{R}^L$.

For any $1 \leq s, t \leq M$, $t > s$,

$$\begin{aligned}
(\mathbf{B}^\top \mathbf{B})_{st} &= \sum_{m=1}^M (\mathbf{P}_m \mathbf{w} \mathbf{w}^\top \mathbf{P}_m^\top)_{st} \\
&= \sum_{m=1}^M (\mathbf{P}_m \mathbf{w})_s (\mathbf{P}_m \mathbf{w})_t \\
&= \sum_{a \in \{|\mathbf{w}_i|\} - \{0\}} a \sum_{m: (\mathbf{P}_m \mathbf{w})_s = a} (\mathbf{P}_m \mathbf{w})_t \\
&= \sum_{a \in \{|\mathbf{w}_i|\} - \{0\}} ab(a),
\end{aligned} \tag{13}$$

and for any $s = t$

$$\begin{aligned}
(\mathbf{B}^\top \mathbf{B})_{ss} &= \sum_{m=1}^M (\mathbf{P}_m \mathbf{w})_s^2 \\
&= \sum_{a \in \{|\mathbf{w}_i|\} - \{0\}} a \sum_{m: |\mathbf{P}_m \mathbf{w}|_s = a} |\mathbf{P}_m \mathbf{w}|_s \\
&= \sum_{a \in \{|\mathbf{w}_i|\} - \{0\}} ad(a).
\end{aligned} \tag{14}$$

It means that for any s, t , $(\mathbf{B}^\top \mathbf{B})_{st}$ is a constant.

Denote $x = (\mathbf{B}^\top \mathbf{B})_{ss}$ and $y = (\mathbf{B}^\top \mathbf{B})_{st}$, $s \neq t$. Then we have $\mathbf{B}^\top \mathbf{B} = (x - y)\mathbf{I} + y\mathbf{1}\mathbf{1}^\top$.

Hence,

$$\begin{aligned}
&(\mathbf{B}\mathbf{B}^\top \mathbf{B})_{r:} \\
&= \mathbf{B}_{r:} \mathbf{B}^\top \mathbf{B} \\
&= \mathbf{w}^\top \mathbf{P}_r^\top ((x - y)\mathbf{I} + y\mathbf{1}\mathbf{1}^\top) \\
&= (x - y)\mathbf{B}_{r:}.
\end{aligned}$$

We finish the necessity part.

Conversely, since $\mathbf{1}^\top \mathbf{P}_m \mathbf{w} = \mathbf{B}_{r:} \mathbf{1} = 0$ for any m , we have

$$\begin{aligned}
(\mathbf{B}\mathbf{B}^\top \mathbf{B})_{r:} &= \mathbf{B}_{r:} \mathbf{B}^\top \mathbf{B} = c_1 \mathbf{B}_{r:} \\
&= \mathbf{B}_{r:} (c_1 \mathbf{I} + c_2 \mathbf{1}\mathbf{1}^\top).
\end{aligned}$$

Let c_2 be $-c_1/L$. Then $\mathbf{1}^\top (c_1 \mathbf{I} + c_2 \mathbf{1}\mathbf{1}^\top) = c_1 \mathbf{1}^\top + c_2 L \mathbf{1}^\top = \mathbf{0}^\top$. Hence $\text{span}\{\mathbf{1}, \mathbf{B}_{r:}^\top, r = 1, \dots, M\} = \mathbb{R}^L$ and thus $\mathbf{B}^\top \mathbf{B} \mathbf{x} = (c_1 \mathbf{I} + c_2 \mathbf{1}\mathbf{1}^\top) \mathbf{x}$ for any $\mathbf{x} \in \mathbb{R}^L$. Together with the observation in Equations (13) and (14), we complete the proof. \square

Proof of Corollary 3.3. The proof of Proposition 3.2 implies that $\mathbf{B}^\top \mathbf{B} = c\mathbf{I} - \frac{c}{L}\mathbf{1}\mathbf{1}^\top$. Then, we have

$$\begin{aligned}
\mathbf{P}\mathbf{P}^\top &= \frac{1}{L}\mathbf{1}\mathbf{1}^\top + \frac{1}{c}\mathbf{B}^\top \mathbf{B} \\
&= \frac{1}{L}\mathbf{1}\mathbf{1}^\top + \mathbf{I} - \frac{1}{L}\mathbf{1}\mathbf{1}^\top = \mathbf{I}.
\end{aligned}$$

We complete the proof. \square

Proof of Corollary 3.4. We only need to show that $\mathbf{B}_\Lambda, \mathbf{p}_\Lambda$ satisfy $\mathbf{B}_\Lambda \mathbf{B}_\Lambda^\top \mathbf{B}_\Lambda = \mathbf{B}_\Lambda$, $\mathbf{B}_\Lambda \mathbf{p}_\Lambda = \mathbf{0}$ and $\text{Rank}(\mathbf{B}_\Lambda) = L_\Lambda - 1$. Obviously, $\mathbf{B}_\Lambda \mathbf{p}_\Lambda = \mathbf{0}$. Define $\mathbf{A}_\Lambda := [\mathbf{p}_\Lambda, \mathbf{B}_\Lambda^\top]^\top$. By direct evaluations, one can show that the columns of \mathbf{A}_Λ satisfy $\|[\mathbf{A}_\Lambda]_{:\ell_1}\| = 1$ and $\langle [\mathbf{A}_\Lambda]_{:\ell_1}, [\mathbf{A}_\Lambda]_{:\ell_2} \rangle = 0$ for all $\ell_1 \neq \ell_2$. That is, $\mathbf{A}_\Lambda^\top \mathbf{A}_\Lambda = \mathbf{I}$, where \mathbf{I} is the identity matrix of size L_Λ . Consequently, we deduce that $\mathbf{B}_\Lambda^\top \mathbf{B}_\Lambda = \mathbf{A}_\Lambda^\top \mathbf{A}_\Lambda - \mathbf{p}_\Lambda \mathbf{p}_\Lambda^\top = \mathbf{I} - \mathbf{p}_\Lambda \mathbf{p}_\Lambda^\top$, which then implies $\mathbf{B}_\Lambda \mathbf{B}_\Lambda^\top \mathbf{B}_\Lambda = \mathbf{B}_\Lambda (\mathbf{I} - \mathbf{p}_\Lambda \mathbf{p}_\Lambda^\top) = \mathbf{B}_\Lambda$ in view of $\mathbf{B}_\Lambda \mathbf{p}_\Lambda = \mathbf{0}$. Now $\text{Rank}(\mathbf{B}_\Lambda) = L_\Lambda - 1$ directly follows from that \mathbf{A}_Λ is of full column rank and $\mathbf{B}_\Lambda \mathbf{p}_\Lambda = \mathbf{0}$. We are done. \square

Algorithm 3 Generating framelets

Input: Node set \mathcal{V} , Partition \mathcal{P}_K , Vectors $\{\mathbf{p}_\Lambda\}$, Matrices $\{\mathbf{B}_\Lambda\}$, j_0
 initialize $\mathcal{F}_{j_0}(\mathcal{P}_K) = \emptyset$, $\phi_\Lambda = \mathbf{I}_{:i}$ for any $s_\Lambda = \{i\}$.
for $j = 2$ **to** $j_0 - 1$ **do**
for $\Lambda \in \{\Lambda : \dim(\Lambda) = j\}$ **do**
 $\phi_\Lambda := \sum_{\ell \in [L_\Lambda]} p_{(\Lambda, \ell)} \phi_{(\Lambda, \ell)}$
for $m = 1$ **to** M_Λ **do**
 $\psi_{(\Lambda, m)} := \sum_{\ell \in [L_\Lambda]} (\mathbf{B}_\Lambda)_{m, \ell} \phi_{(\Lambda, \ell)}$
 update $\mathcal{F}_{j_0}(\mathcal{P}_K) \leftarrow \mathcal{F}_{j_0}(\mathcal{P}_K) \cup \{\phi_\Lambda, \psi_{(\Lambda, m), m=1, \dots, M_\Lambda}\}$
Output: $\mathcal{F}_{j_0}(\mathcal{P}_K)$

For generating framelets, we use Algorithm 3 (Equations (1) and (2)). Its efficiency is discussed in Theorem 3.7.

Proof of Theorem 3.7. Denote \mathbf{F} the framelet matrix in which each column is the element of $\mathcal{F}_{j_0}(\mathcal{P}_K) = \{\phi_\Lambda : \dim(\Lambda) = j_0\} \cup \{\psi_\Lambda : \dim(\Lambda) = j_0 + 1, \dots, K\}$.

We first consider the sparsity of $\langle \mathbf{I}_{:1}, \psi_{(\Lambda, m)} \rangle$, $m = 1, \dots, M_\Lambda$. Notice that only when the node $1 \in s_\Lambda$, can the term $\langle \mathbf{I}_{:1}, \psi_{(\Lambda, m)} \rangle$ be nonzero. Thus, without loss of generality, we can assume that $1 \in s_\Lambda$. By the matrix \mathbf{B}_Λ we define, we see that $\psi_{(\Lambda, m)} = \frac{1}{\sqrt{L_\Lambda}} (\phi_{(\Lambda, \ell_1)} - \phi_{(\Lambda, \ell_2)})$ for the unique pair $m = m(\ell_1, \ell_2) = m(\ell_1, \ell_2, L_\Lambda)$ satisfying $1 \leq \ell_1 < \ell_2 \leq L_\Lambda$ as given in Corollary 3.4. Again, only when the support of $\phi_{(\Lambda, \ell_1)}$ or $\phi_{(\Lambda, \ell_2)}$ contains 1, can the inner product $\langle \mathbf{I}_{:1}, \psi_{(\Lambda, m)} \rangle$ be nonzero.

Now we count the total number of such pairs (ℓ_1, ℓ_2) with (ℓ_1, ℓ_2) mapped to m so that $\psi_{(\Lambda, m)} = \frac{1}{\sqrt{L_\Lambda}} (\phi_{(\Lambda, \ell_1)} - \phi_{(\Lambda, \ell_2)})$ with either $s_{(\Lambda, \ell_1)}$ or $s_{(\Lambda, \ell_2)}$ containing the node 1. Since $1 \in s_\Lambda$ and $\{s_{(\Lambda, \ell_1)} : \ell_1 \in [L_\Lambda]\}$ form a partition of s_Λ , we see that there exists exactly one $\ell_0 \in [L_\Lambda]$ such that $1 \in s_{\Lambda, \ell_0}$. Then, we see that only those m with (ℓ_0, ℓ_2) mapped to m for $\ell_2 = \ell_0 + 1, \dots, L_\Lambda$ or m with (ℓ_2, ℓ_0) mapped to m for $\ell_2 = 1, \dots, \ell_0 - 1$ can make the term $\langle \mathbf{I}_{:1}, \psi_{(\Lambda, m)} \rangle$ being nonzero. The total number of such m is $L_\Lambda - 1 \leq h - 1$. Thus, at most $h - 1$ framelets $\psi_{(\Lambda, m)}$ that make $\langle \mathbf{I}_{:1}, \psi_{(\Lambda, m)} \rangle \neq 0$.

For each j , only one cluster s_Λ of $\mathcal{V}_j = \{\Lambda : \dim(\Lambda) = j\}$ contains node 1. Thus $\mathbf{F}^\top \mathbf{I}_{:1}$ has at most $(h - 1)(K - 1)$ nonzero entries. Similar results hold for $\mathbf{I}_{:i}$. Hence, for $\mathbf{f} = [f_1, \dots, f_n]^\top$, it is easy to show that $\|\hat{\mathbf{f}}\|_0 = \|\mathbf{F}^\top \mathbf{f}\|_0 = \|\sum_{i \in [n], f_i \neq 0} \mathbf{F}^\top \mathbf{I}_{:i}\|_0 \leq \sum_{i \in [n], f_i \neq 0} \|\mathbf{F}^\top \mathbf{I}_{:i}\|_0 \leq (h - 1)(K - 1)\|\mathbf{f}\|_0$. \square

Proof of Theorem 3.9. Note that we have $n \leq Ch^{K-1}$ and $\#\mathcal{V}_j = \#\{\Lambda : \dim(\Lambda) = j\} \leq Ch^{j-1}$ for some fixed constant $C > 0$. Note that we have

$$M_\Lambda = \frac{L_\Lambda(L_\Lambda - 1)}{2} \leq \frac{h(h - 1)}{2}.$$

Therefore, there is no more than

$$C(h^{j_0-1} + \sum_{j=j_0}^{K-1} \frac{1}{2} h(h - 1)h^{j-1}) = O(nh)$$

elements in the binary graph Haar framelet system $\mathcal{F}_{j_0}(\mathcal{P}_K)$ for any $j_0 \in [K]$.

By Equations (1) and (2), we have

$$\phi_\Lambda^\top := \mathbf{p}_\Lambda^\top \begin{bmatrix} \phi_{(\Lambda, 1)}^\top \\ \vdots \\ \phi_{(\Lambda, L_\Lambda)}^\top \end{bmatrix}, \quad \begin{bmatrix} \psi_{(\Lambda, 1)}^\top \\ \vdots \\ \psi_{(\Lambda, M_\Lambda)}^\top \end{bmatrix} := \mathbf{B}_\Lambda \begin{bmatrix} \phi_{(\Lambda, 1)}^\top \\ \vdots \\ \phi_{(\Lambda, L_\Lambda)}^\top \end{bmatrix}, \quad (15)$$

By our construction, there is at most h^{K-j} nonzero entries for each ϕ_Λ and at most $2 \cdot h^{K-j-1}$ nonzero entries for each $\psi_{(\Lambda, m)}$ for $\dim(\Lambda) = j$. Hence, the number of nonzeros entries of \mathbf{F} is at most

$$C(h^{K-j_0} \cdot h^{j_0-1} + \sum_{j=j_0}^{K-1} 2h^{K-j-1} \cdot \frac{h(h - 1)}{2} \cdot h^{j-1}) \leq C(K - 1)h^K = O(nh \log_h n)$$

Fix a Λ which has size $\dim(\Lambda) = j$. Then Equation (17) implies at most $h \cdot h^{K-j-1}$ multiplication operations and $(h-1) \cdot h^{K-j-1}$ addition operations needed for ϕ_Λ . For computing $\Psi_{(\Lambda,m)}$, $m = 1, \dots, M_\Lambda$, we need at most $2 \cdot h^{K-j-1} \cdot \frac{h(h-1)}{2}$ multiplication operations and $h^{K-j-1} \cdot \frac{h(h-1)}{2}$ addition operations, respectively. Notice that $\#\mathcal{V}_j \leq Ch^{j-1}$. To compute the nonzero entries of ϕ_Λ and $\psi_{(\Lambda,m)}$ for all $\dim(\Lambda) = j$ and $m = 1, \dots, M_\Lambda$, from the above computation, one can see that it needs at most

$$2C \left(h^{K-j-1} \cdot h \cdot h^{j-1} + 2h^{K-j-1} \cdot \frac{h(h-1)}{2} \cdot h^{j-1} \right) = 2C \cdot h^K$$

evaluations of multiplications and additions. Hence, in total, to compute the nonzero entries of ϕ_Λ and $\psi_{(\Lambda,m)}$ for all $\dim(\Lambda) = j_0, \dots, K-1$ and $m = 1, \dots, M_\Lambda$, it needs at most

$$2C \sum_{j=1}^{K-1} \left(h^{K-j-1} \cdot h \cdot h^{j-1} + 2h^{K-j-1} \cdot \frac{h(h-1)}{2} \cdot h^{j-1} \right) = 2C(K-1)h^K = O(nh \log_h n)$$

evaluations of multiplications and additions. \square

Before showing the proof of Theorem 3.11, we want to give some comments on permutations. Notice that the construction of \mathbf{p}_Λ and \mathbf{B}_Λ only depends on L_Λ . Hence, under node permutation (π or \mathbf{P}_π), it means that we have the following relationship between original ϕ_Λ and ϕ_Λ^* , ψ_Λ and ψ_Λ^* ,

$$(\phi_\Lambda^*)^\top := \mathbf{p}_\Lambda^\top \begin{bmatrix} \phi_{(\Lambda,1)}^\top \\ \vdots \\ \phi_{(\Lambda,L_\Lambda)}^\top \end{bmatrix} \mathbf{P}_\pi, \quad \begin{bmatrix} (\psi_{(\Lambda,1)}^*)^\top \\ \vdots \\ (\psi_{(\Lambda,M_\Lambda)}^*)^\top \end{bmatrix} := \mathbf{B}_\Lambda \begin{bmatrix} \phi_{(\Lambda,1)}^\top \\ \vdots \\ \phi_{(\Lambda,L_\Lambda)}^\top \end{bmatrix} \mathbf{P}_\pi. \quad (16)$$

Under partition permutation π_p , fixing a Λ (there exists a permutation matrix \mathbf{Q}_Λ w.r.t. π_p at Λ), we have the following relationship between original ϕ_Λ and ϕ_Λ^* , ψ_Λ and ψ_Λ^* ,

$$(\phi_\Lambda^*)^\top := \mathbf{p}_\Lambda^\top \mathbf{Q}_\Lambda \begin{bmatrix} \phi_{(\Lambda,1)}^\top \\ \vdots \\ \phi_{(\Lambda,L_\Lambda)}^\top \end{bmatrix}, \quad \begin{bmatrix} (\psi_{(\Lambda,1)}^*)^\top \\ \vdots \\ (\psi_{(\Lambda,M_\Lambda)}^*)^\top \end{bmatrix} := \mathbf{B}_\Lambda \mathbf{Q}_\Lambda \begin{bmatrix} \phi_{(\Lambda,1)}^\top \\ \vdots \\ \phi_{(\Lambda,L_\Lambda)}^\top \end{bmatrix}. \quad (17)$$

Proof of Theorem 3.11. Let $\Phi_\Lambda := [\phi_{(\Lambda,1)}, \dots, \phi_{(\Lambda,L_\Lambda)}]^\top$ and $\Psi_\Lambda := [\psi_{(\Lambda,1)}, \dots, \psi_{(\Lambda,M_\Lambda)}]^\top$. Since the scaling vectors $\phi_\Lambda^\top = \mathbf{p}_\Lambda^\top \Phi_\Lambda$ are defined iteratively for $\dim(\Lambda)$ decreasing from K to 1 through Equation (1) and the framelets $\psi_{(\Lambda,m)}$ are given by $\Psi_\Lambda = \mathbf{B}_\Lambda \Phi_\Lambda$, we only need to prove the permutation equivariance properties for each Λ .

For Item (i), note that by Equation (1) and Corollary 3.4, $\phi_{(\Lambda,\ell)} : \mathcal{V} \rightarrow \mathbb{R}$ only depends on $\mathcal{G}, \mathcal{P}_K$, and $\mathbf{p}_\Lambda = \frac{1}{\sqrt{L_\Lambda}} \mathbf{1}$. For any node permutation π , the \mathcal{P}_K is determined by the index vectors Λ according to a tree structure and is independent of the node permutation π . Moreover, the vectors \mathbf{p}_Λ are fixed constants. Hence, iteratively, after node permutation π acting on graph \mathcal{G} , the new scaling vector $\phi_{(\Lambda,\ell)}^\pi : \pi(\mathcal{V}) \rightarrow \mathbb{R}$ is given by $\phi_{(\Lambda,\ell)}^\pi = \mathbf{P}_\pi \phi_{(\Lambda,\ell)}$, where \mathbf{P}_π is the permutation matrix with respect to π . Consequently, the new Φ_Λ^π and Ψ_Λ^π on the permuted graph $\pi(\mathcal{G})$ are given by $\Phi_\Lambda^\pi = \Phi_\Lambda \mathbf{P}_\pi$ and $\Psi_\Lambda^\pi = \mathbf{B}_\Lambda \Phi_\Lambda^\pi = \mathbf{B}_\Lambda \Phi_\Lambda \mathbf{P}_\pi = \Psi_\Lambda \mathbf{P}_\pi$. This implies the conclusion in Item (i).

For Item (ii), given a partition permutation π_p acting on \mathcal{P}_K , We denote $\pi_p(\mathcal{P}_K)$ the hierarchical clustering w.r.t. such a π_p . Let $\tilde{\Lambda} := \pi_p(\Lambda)$ be the permuted index vector $\pi_p(\mathcal{P}_K)$ from the index vector Λ in \mathcal{P}_K . Since the partition permutation acts on the children of each Λ only, we have $\pi_p(\Lambda, \ell) = (\tilde{\Lambda}, \pi_\Lambda(\ell))$ for some permutation π_Λ on $[L_\Lambda]$. Then, the matrix $\Phi_{\tilde{\Lambda}}$ is

$$\Phi_{\tilde{\Lambda}} := [\phi_{(\tilde{\Lambda},\pi_\Lambda(1))}, \dots, \phi_{(\tilde{\Lambda},\pi_\Lambda(L_\Lambda))}]^\top = \mathbf{P}_{\pi_\Lambda} \Phi_\Lambda$$

with \mathbf{P}_{π_Λ} being the permutation matrix with respect to π_Λ . Then, in view of $\mathbf{p}_\Lambda^\top \mathbf{P}_{\pi_\Lambda} = \mathbf{p}_\Lambda^\top$, the permuted scaling vector $\phi_{\tilde{\Lambda}}$ is given by

$$(\phi_{\tilde{\Lambda}})^\top = (\phi_{\pi_p(\Lambda)})^\top = \mathbf{p}_\Lambda^\top (\mathbf{P}_{\pi_\Lambda} \Phi_\Lambda) = (\mathbf{p}_\Lambda^\top \mathbf{P}_{\pi_\Lambda}) \Phi_\Lambda = \mathbf{p}_\Lambda^\top \Phi_\Lambda = \phi_\Lambda^\top,$$

That is, the new scaling vectors in $\{\phi_{\tilde{\Lambda}} : \dim(\tilde{\Lambda}) = j\}$ are simply the recording of $\{\phi_\Lambda : \dim(\Lambda) = j\}$ under π_p for $j = 0, \dots, K$. Thus, all scaling vectors are invariant (up to index permutation) under the partition permutation π_p . Now for the framelet vectors $\psi_{(\Lambda,m)}$, by Equation (2), we have

$$\Psi_{\tilde{\Lambda}} = \mathbf{B}_\Lambda \Phi_{\tilde{\Lambda}} = \mathbf{B}_\Lambda \mathbf{P}_{\pi_\Lambda} \Phi_\Lambda.$$

We claim that there exist $M_\Lambda \times M_\Lambda$ permutation matrix \mathbf{R}_Λ and sign matrix $\mathbf{S}_\Lambda = \text{diag}(c_1, \dots, c_{M_\Lambda})$ with all $c_i \in \{-1, +1\}$ such that $\mathbf{B}_\Lambda \mathbf{P}_{\pi_\Lambda} = \mathbf{S}_\Lambda \mathbf{R}_\Lambda \mathbf{B}_\Lambda$. Then, we have

$$\Psi_{\tilde{\Lambda}} = \mathbf{B}_\Lambda \mathbf{P}_{\pi_\Lambda} \Phi_\Lambda = \mathbf{S}_\Lambda \mathbf{R}_\Lambda \mathbf{B}_\Lambda \Phi_\Lambda = \mathbf{S}_\Lambda \mathbf{R}_\Lambda \Psi_\Lambda,$$

which then concludes Item (ii). Noting that $\mathbf{B}_\Lambda \mathbf{P}_{\pi_\Lambda}$ is to reorder the columns of \mathbf{B}_Λ and regardless the sign, all elements appear in each column with the same times and 1 (or -1) appears in rows of \mathbf{B}_Λ once. In other words, $(\mathbf{B}_\Lambda \mathbf{P}_{\pi_\Lambda})_{r:} = \mathbf{w}^\top \mathbf{P}_r^\top \mathbf{P}_{\pi_\Lambda}$, which is to permute $\mathbf{w} = [1, -1, 0, \dots, 0]^\top$ (up to a constant) with respect to $\mathbf{P}_r^\top \mathbf{P}_{\pi_\Lambda}$. Since $\text{Rank}(\mathbf{B}_\Lambda) = L - 1$ and $\mathbf{B}_\Lambda \mathbf{1} = \mathbf{0}$, we have $\mathbf{P}\mathbf{w} \in \text{span}\{\mathbf{P}_m \mathbf{w}\}_{m=1}^{M_\Lambda}$ for any permutation matrix \mathbf{P} . Thus for any r , there exists exactly one $j \in [M_\Lambda]$ such that $(\mathbf{B}_\Lambda \mathbf{P}_{\pi_\Lambda})_{r:} = \mathbf{w}^\top \mathbf{P}_r^\top \mathbf{P}_{\pi_\Lambda} = c \mathbf{w}^\top \mathbf{P}_j^\top$ where c is either 1 or -1 . Hence the claim holds. This completes the proof of Item (ii).

The proof of Item (iii) is a direct consequence of Items (i) and (ii). \square

Proof of Proposition 4.1. From Theorem 3.11 (i), we know that the corresponding permuted versions of Φ_1 and Ψ_j are $\Phi_1 \mathbf{P}$ and $\Psi_j \mathbf{P}$. Thus $\mathbf{F}_j(\mathbf{P}\mathbf{X}) = \mathbf{P}\mathbf{F}_j(\mathbf{X})$, $\mathbf{F}_j(\mathbf{P}\mathbf{A}\mathbf{P}^\top \mathbf{P}\mathbf{X}) = \mathbf{P}\mathbf{F}_j(\mathbf{A}\mathbf{X})$, $\mathbf{F}_j(\mathbf{P}\tilde{\mathbf{A}}\mathbf{P}^\top \mathbf{P}\mathbf{X}) = \mathbf{P}\mathbf{F}_j(\tilde{\mathbf{A}}\mathbf{X})$ for $j = 0, \dots, K - 1$. It is obvious that the remaining channels also differ by a permutation matrix \mathbf{P} . Since the row normalization and the softmax function are applied row-wise and the activation function is applied element-wise, it is straightforward to see that $\hat{\mathbf{Y}}_P = \mathbf{P}\hat{\mathbf{Y}}$. \square

B Fast Decomposition and Reconstruction Algorithms

Proof of Theorem 3.6. A fast decomposition algorithm is given by Equation (5), which computes $\hat{\mathbf{f}}$ iteratively. In order to get x_Λ and $y_{(\Lambda, m)}$ for $\hat{\mathbf{f}}$, we need to compute $\sum_{\ell \in [L_\Lambda]} x_{(\Lambda, \ell)} (\mathbf{C}_\Lambda)_{\ell, t} = (\mathbf{q}_\Lambda^\top \mathbf{C}_\Lambda)_t$, where $t = 1, \dots, M_\Lambda + 1$, $\ell \in [L_\Lambda]$ and $\mathbf{q}_\Lambda := [x_{(\Lambda, 1)}, \dots, x_{(\Lambda, L_\Lambda)}]^\top$ (see Equation (6)). Note that for our binary graph Haar framelet system $\mathcal{F}_{j_0}(\mathcal{P}_K)$, the matrix \mathbf{C}_Λ in Equation (4) is given by $\mathbf{C}_\Lambda = [\mathbf{p}_\Lambda, \mathbf{B}_\Lambda^\top]$ and each row of \mathbf{B}_Λ has only two nonzero elements. Hence, for a given Λ with $\dim(\Lambda) = j$, since $L_\Lambda \leq h$ and $M_\Lambda \leq \frac{h(h-1)}{2}$, the number of nonzero elements in \mathbf{C}_Λ is no more than $h + 2 \cdot \frac{h(h-1)}{2}$. Therefore, the computational complexity for obtaining $\mathbf{q}_\Lambda^\top \mathbf{C}$ is of the same order as $h + 2 \cdot \frac{h(h-1)}{2}$. In total, observing that $\#\{\Lambda : \dim(\Lambda) = j\} \leq h^{j-1}$, to get the full $\hat{\mathbf{f}}$, the computational complexity is of order the same as $\sum_{j=1}^{K-1} (h + 2 \cdot \frac{h(h-1)}{2}) h^{j-1} = O(nh)$.

Fast reconstruction algorithm (Equation (7)) which computes \mathbf{f} from $\hat{\mathbf{f}}$ only need to compute \mathbf{r}_Λ iteratively. Let $\mathbf{Y}_\Lambda := [x_\Lambda, \mathbf{y}_\Lambda^\top]^\top \in \mathbb{R}^{M_\Lambda + 1}$ and $\mathbf{P}_\Lambda := \begin{pmatrix} \mathbf{p}_\Lambda^\top \\ \mathbf{B}_\Lambda^\top \end{pmatrix}$. Then $\mathbf{P}_\Lambda = \mathbf{C}_\Lambda^\top$ and $\mathbf{r}_\Lambda = \mathbf{Y}_\Lambda^\top \mathbf{P}_\Lambda$. Following a similar calculation as for the fast decomposition algorithm, it is not hard to see the computation complexity is of $\sum_{j=1}^{K-1} h^{j-1} (h + 2 \cdot \frac{h(h-1)}{2}) = O(nh)$. \square

C Examples of Binary Haar Graph Framelets

For simplicity, we denote $\Phi_\Lambda = [\phi_{(\Lambda, 1)}, \dots, \phi_{(\Lambda, L_\Lambda)}]$ and $\Psi_\Lambda = [\psi_{(\Lambda, 1)}, \dots, \psi_{(\Lambda, M_\Lambda)}]$ throughout this section. In Example 1 (Figure 5), we are given a path graph \mathcal{G}_1 with 8 nodes $\mathcal{V} = \{1, 2, \dots, 8\}$. We choose hierarchical clustering $\mathcal{P}_4 = \{\mathcal{V}_1, \mathcal{V}_2, \mathcal{V}_3, \mathcal{V}_4\}$ with

$$\begin{aligned} \mathcal{V}_1 &= \{s_{(1)}\}, \\ \mathcal{V}_2 &= \{s_{(1,1)}, s_{(1,2)}\}, \\ \mathcal{V}_3 &= \{s_{(1,1,1)}, s_{(1,1,2)}, s_{(1,2,1)}, s_{(1,2,2)}\}, \\ \mathcal{V}_4 &= \{s_{(1,1,1,1)}, s_{(1,1,1,2)}, s_{(1,1,2,1)}, s_{(1,1,2,2)}, \\ &\quad s_{(1,2,1,1)}, s_{(1,2,1,2)}, s_{(1,2,2,1)}, s_{(1,2,2,2)}\}, \end{aligned}$$

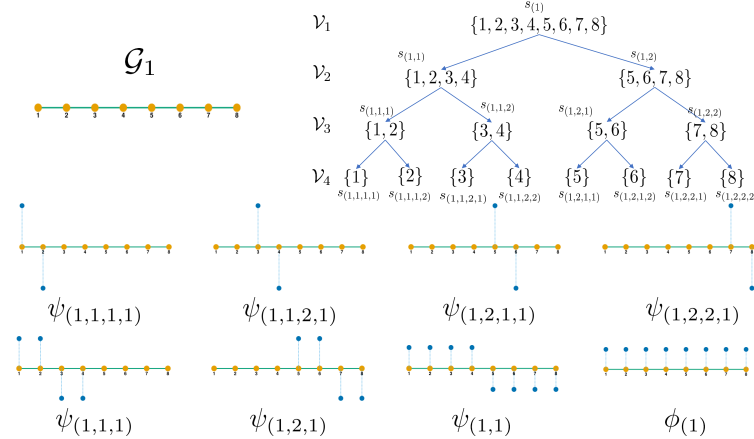


Figure 5: Graph framelet on \mathcal{G}_1 with partition \mathcal{P}_4 .

and $\mathbf{p}_\Lambda = [\frac{1}{\sqrt{2}}, \frac{1}{\sqrt{2}}]^\top$ and $\mathbf{B}_\Lambda = [\frac{1}{\sqrt{2}}, -\frac{1}{\sqrt{2}}]$ for all Λ . It is obvious that $L_\Lambda = 2$ and $M_\Lambda = 1$. When the dimension $\dim(\Lambda) = 3$, we have $\Lambda \in \{(1, 1, 1), (1, 1, 2), (1, 2, 1), (1, 2, 2)\}$ and

Then by definition, we obtain

$$\begin{aligned}\phi_{(1,1,1)}^\top &= p_{(1,1,1)}^\top \Phi_{(1,1,1)}^\top = \begin{bmatrix} \frac{1}{\sqrt{2}} & \frac{1}{\sqrt{2}} & 0 & 0 & 0 & 0 & 0 & 0 \end{bmatrix}, \\ \phi_{(1,1,2)}^\top &= p_{(1,1,2)}^\top \Phi_{(1,1,2)}^\top = \begin{bmatrix} 0 & 0 & \frac{1}{\sqrt{2}} & \frac{1}{\sqrt{2}} & 0 & 0 & 0 & 0 \end{bmatrix}, \\ \phi_{(1,2,1)}^\top &= p_{(1,2,1)}^\top \Phi_{(1,2,1)}^\top = \begin{bmatrix} 0 & 0 & 0 & 0 & \frac{1}{\sqrt{2}} & \frac{1}{\sqrt{2}} & 0 & 0 \end{bmatrix}, \\ \phi_{(1,2,2)}^\top &= p_{(1,2,2)}^\top \Phi_{(1,2,2)}^\top = \begin{bmatrix} 0 & 0 & 0 & 0 & 0 & 0 & \frac{1}{\sqrt{2}} & \frac{1}{\sqrt{2}} \end{bmatrix},\end{aligned}$$

and

$$\begin{aligned}\Psi_{(1,1,1)}^\top &= \mathbf{B}_{(1,1,1)} \Phi_{(1,1,1)}^\top = \begin{bmatrix} \frac{1}{\sqrt{2}} & -\frac{1}{\sqrt{2}} & 0 & 0 & 0 & 0 & 0 & 0 \end{bmatrix}, \\ \Psi_{(1,1,2)}^\top &= \mathbf{B}_{(1,1,2)} \Phi_{(1,1,2)}^\top = \begin{bmatrix} 0 & 0 & \frac{1}{\sqrt{2}} & -\frac{1}{\sqrt{2}} & 0 & 0 & 0 & 0 \end{bmatrix}, \\ \Psi_{(1,2,1)}^\top &= \mathbf{B}_{(1,2,1)} \Phi_{(1,2,1)}^\top = \begin{bmatrix} 0 & 0 & 0 & 0 & \frac{1}{\sqrt{2}} & -\frac{1}{\sqrt{2}} & 0 & 0 \end{bmatrix}, \\ \Psi_{(1,2,2)}^\top &= \mathbf{B}_{(1,2,2)} \Phi_{(1,2,2)}^\top = \begin{bmatrix} 0 & 0 & 0 & 0 & 0 & 0 & \frac{1}{\sqrt{2}} & -\frac{1}{\sqrt{2}} \end{bmatrix}.\end{aligned}$$

Similarly, when $\dim(\Lambda) = 2$, or equivalently, $\Lambda \in \{(1, 1), (1, 2)\}$, we can get

$$\begin{aligned}\boldsymbol{\phi}_{(1,1)}^\top &= \boldsymbol{p}_{(1,1)}^\top \boldsymbol{\Phi}_{(1,1)}^\top = \boldsymbol{p}_{(1,1)}^\top [\boldsymbol{\phi}_{(1,1,1)}, \boldsymbol{\phi}_{(1,1,2)}]^\top = \left[\frac{1}{2} \quad \frac{1}{2} \quad \frac{1}{2} \quad \frac{1}{2} \quad 0 \quad 0 \quad 0 \quad 0 \right], \\ \boldsymbol{\phi}_{(1,2)}^\top &= \boldsymbol{p}_{(1,2)}^\top \boldsymbol{\Phi}_{(1,2)}^\top = \boldsymbol{p}_{(1,2)}^\top [\boldsymbol{\phi}_{(1,2,1)}, \boldsymbol{\phi}_{(1,2,2)}]^\top = \left[0 \quad 0 \quad 0 \quad 0 \quad \frac{1}{2} \quad \frac{1}{2} \quad \frac{1}{2} \quad \frac{1}{2} \right],\end{aligned}$$

and

$$\begin{aligned}\Psi_{(1,1)}^\top &= \mathbf{B}_{(1,1)} \Phi_{(1,1)}^\top = \mathbf{B}_{(1,1)} [\phi_{(1,1,1)}, \phi_{(1,1,2)}]^\top = \left[\frac{1}{2} \quad \frac{1}{2} \quad -\frac{1}{2} \quad -\frac{1}{2} \quad 0 \quad 0 \quad 0 \quad 0 \right], \\ \Psi_{(1,2)}^\top &= \mathbf{B}_{(1,2)} \Phi_{(1,2)}^\top = \mathbf{B}_{(1,2)} [\phi_{(1,2,1)}, \phi_{(1,2,2)}]^\top = \left[0 \quad 0 \quad 0 \quad 0 \quad \frac{1}{2} \quad \frac{1}{2} \quad -\frac{1}{2} \quad -\frac{1}{2} \right].\end{aligned}$$

And when $\dim(\Lambda) = 1$, or equivalently, $\Lambda \in \{(1)\}$, we can get

$$\phi_{(1)}^\top = \mathbf{p}_{(1)}^\top \Phi_{(1)}^\top = \mathbf{p}_{(1)}^\top [\phi_{(1,1)}, \phi_{(1,2)}]^\top = \left[\frac{1}{2\sqrt{2}} \quad \frac{1}{2\sqrt{2}} \quad \frac{1}{2\sqrt{2}} \quad \frac{1}{2\sqrt{2}} \quad \frac{1}{2\sqrt{2}} \quad \frac{1}{2\sqrt{2}} \quad \frac{1}{2\sqrt{2}} \right],$$

and

$$\Psi_{(1)}^\top = \mathbf{B}_{(1)} \Phi_{(1)}^\top = \mathbf{B}_{(1)} [\phi_{(1,1)}, \phi_{(1,2)}]^\top = \left[\frac{1}{2\sqrt{2}} \quad \frac{1}{2\sqrt{2}} \quad \frac{1}{2\sqrt{2}} \quad \frac{1}{2\sqrt{2}} \quad -\frac{1}{2\sqrt{2}} \quad -\frac{1}{2\sqrt{2}} \quad -\frac{1}{2\sqrt{2}} \right].$$

Hence, the framelet system $\{\phi_\Lambda, \dim(\Lambda) = 1\} \cup \{\psi_\Lambda, \dim(\Lambda) > 1\}$ are formed by columns of the following matrix

$$\mathbf{F} := [\Psi_{(1,1,1)}, \Psi_{(1,1,2)}, \Psi_{(1,2,1)}, \Psi_{(1,2,2)}, \Psi_{(1,1)}, \Psi_{(1,2)}, \Psi_{(1)}, \Phi_{(1)}]$$

$$= \begin{bmatrix} \frac{1}{\sqrt{2}} & 0 & 0 & 0 & \frac{1}{2} & 0 & \frac{1}{2\sqrt{2}} & \frac{1}{2\sqrt{2}} \\ -\frac{1}{\sqrt{2}} & 0 & 0 & 0 & \frac{1}{2} & 0 & \frac{1}{2\sqrt{2}} & \frac{1}{2\sqrt{2}} \\ 0 & \frac{1}{\sqrt{2}} & 0 & 0 & -\frac{1}{2} & 0 & \frac{1}{2\sqrt{2}} & \frac{1}{2\sqrt{2}} \\ 0 & -\frac{1}{\sqrt{2}} & 0 & 0 & -\frac{1}{2} & 0 & \frac{1}{2\sqrt{2}} & \frac{1}{2\sqrt{2}} \\ 0 & 0 & \frac{1}{\sqrt{2}} & 0 & 0 & \frac{1}{2} & -\frac{1}{2\sqrt{2}} & \frac{1}{2\sqrt{2}} \\ 0 & 0 & -\frac{1}{\sqrt{2}} & 0 & 0 & \frac{1}{2} & -\frac{1}{2\sqrt{2}} & \frac{1}{2\sqrt{2}} \\ 0 & 0 & 0 & \frac{1}{\sqrt{2}} & 0 & -\frac{1}{2} & -\frac{1}{2\sqrt{2}} & \frac{1}{2\sqrt{2}} \\ 0 & 0 & 0 & -\frac{1}{\sqrt{2}} & 0 & -\frac{1}{2} & -\frac{1}{2\sqrt{2}} & \frac{1}{2\sqrt{2}} \end{bmatrix}.$$

It is easy to verify that $\mathbf{F}^\top \mathbf{F} = \mathbf{I}$ and thus it forms a tight frame.

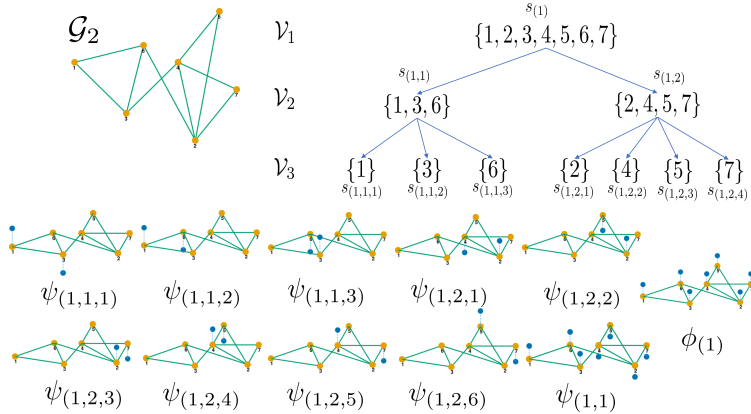


Figure 6: Graph framelet on \mathcal{G}_2 with partition \mathcal{P}_3 .

In Example 2 (Figure 6), according to Corollary 3.4, we choose $\mathbf{p}_{(1,1)} = [\frac{1}{\sqrt{3}}, \frac{1}{\sqrt{3}}, \frac{1}{\sqrt{3}}]^\top$, $\mathbf{p}_{(1,2)} = [\frac{1}{2}, \frac{1}{2}, \frac{1}{2}, \frac{1}{2}]^\top$ and $\mathbf{p}_{(1)} = [\frac{1}{\sqrt{2}}, \frac{1}{\sqrt{2}}]^\top$ for \mathbf{p}_Λ and the following matrices

$$\mathbf{B}_{(1,1)} = \frac{1}{\sqrt{3}} \begin{bmatrix} 1 & -1 & 0 \\ 1 & 0 & -1 \\ 0 & 1 & -1 \end{bmatrix},$$

$$\mathbf{B}_{(1,2)} = \frac{1}{2} \begin{bmatrix} 1 & -1 & 0 & 0 \\ 1 & 0 & -1 & 0 \\ 1 & 0 & 0 & -1 \\ 0 & 1 & -1 & 0 \\ 0 & 1 & 0 & -1 \\ 0 & 0 & 1 & -1 \end{bmatrix},$$

$$\mathbf{B}_{(1)} = \frac{1}{\sqrt{2}} [1 \quad -1].$$

For \mathbf{B}_Λ .

When $\dim(\Lambda) = 2$, or equivalently, $\Lambda \in \{(1, 1), (1, 2)\}$, we obtain

$$\begin{aligned}\boldsymbol{\phi}_{(1,1)}^\top &= \mathbf{p}_{(1,1)}^\top \boldsymbol{\Phi}_{(1,1)}^\top = \mathbf{p}_{(1,1)}^\top [\phi_{(1,1,1)}, \phi_{(1,1,2)}, \phi_{(1,1,3)}]^\top = \begin{bmatrix} \frac{1}{\sqrt{3}} & 0 & \frac{1}{\sqrt{3}} & 0 & 0 & \frac{1}{\sqrt{3}} & 0 \end{bmatrix}, \\ \boldsymbol{\phi}_{(1,2)}^\top &= \mathbf{p}_{(1,2)}^\top \boldsymbol{\Phi}_{(1,2)}^\top = \mathbf{p}_{(1,2)}^\top [\phi_{(1,2,1)}, \phi_{(1,2,2)}, \phi_{(1,2,3)}, \phi_{(1,2,4)}]^\top = \begin{bmatrix} 0 & \frac{1}{2} & 0 & \frac{1}{2} & \frac{1}{2} & 0 & \frac{1}{2} \end{bmatrix},\end{aligned}$$

and

$$\begin{aligned}\boldsymbol{\Psi}_{(1,1)}^\top &= \mathbf{B}_{(1,1)} \boldsymbol{\Phi}_{(1,1)}^\top = \begin{bmatrix} \frac{1}{\sqrt{3}} & 0 & -\frac{1}{\sqrt{3}} & 0 & 0 & 0 & 0 \\ \frac{1}{\sqrt{3}} & 0 & 0 & 0 & 0 & -\frac{1}{\sqrt{3}} & 0 \\ 0 & 0 & \frac{1}{\sqrt{3}} & 0 & 0 & -\frac{1}{\sqrt{3}} & 0 \end{bmatrix}, \\ \boldsymbol{\Psi}_{(1,2)}^\top &= \mathbf{B}_{(1,2)} \boldsymbol{\Phi}_{(1,2)}^\top = \begin{bmatrix} 0 & \frac{1}{2} & 0 & -\frac{1}{2} & 0 & 0 & 0 \\ 0 & \frac{1}{2} & 0 & 0 & -\frac{1}{2} & 0 & 0 \\ 0 & \frac{1}{2} & 0 & 0 & 0 & 0 & -\frac{1}{2} \\ 0 & 0 & 0 & \frac{1}{2} & -\frac{1}{2} & 0 & 0 \\ 0 & 0 & 0 & \frac{1}{2} & 0 & 0 & -\frac{1}{2} \\ 0 & 0 & 0 & 0 & \frac{1}{2} & 0 & -\frac{1}{2} \end{bmatrix}.\end{aligned}$$

When $\dim(\Lambda) = 1$, or equivalently, $\Lambda \in \{(1)\}$, we have

$$\boldsymbol{\phi}_{(1)}^\top = \mathbf{p}_{(1)}^\top \boldsymbol{\Phi}_{(1)}^\top = \mathbf{p}_{(1)}^\top [\phi_{(1,1)}, \phi_{(1,2)}]^\top = \begin{bmatrix} \frac{1}{\sqrt{6}} & \frac{1}{2\sqrt{2}} & \frac{1}{\sqrt{6}} & \frac{1}{2\sqrt{2}} & \frac{1}{2\sqrt{2}} & \frac{1}{\sqrt{6}} & \frac{1}{2\sqrt{2}} \end{bmatrix},$$

and

$$\boldsymbol{\Psi}_{(1)}^\top = \mathbf{B}_{(1)} \boldsymbol{\Phi}_{(1)}^\top = \begin{bmatrix} \frac{1}{\sqrt{6}} & -\frac{1}{2\sqrt{2}} & \frac{1}{\sqrt{6}} & -\frac{1}{2\sqrt{2}} & -\frac{1}{2\sqrt{2}} & \frac{1}{\sqrt{6}} & -\frac{1}{2\sqrt{2}} \end{bmatrix}.$$

Hence, the framelet system $\{\phi_\Lambda, \dim(\Lambda) = 1\} \cup \{\psi_\Lambda, \dim(\Lambda) > 1\}$ are formed by columns of the following matrix

$$\mathbf{F} := [\boldsymbol{\Psi}_{(1,1)}, \boldsymbol{\Psi}_{(1,2)}, \boldsymbol{\Psi}_{(1)}, \boldsymbol{\Phi}_{(1)}].$$

It is easy to verify that $\mathbf{F}^\top \mathbf{F} = \mathbf{I}$ and thus it forms a tight frame.

These two examples are all binary framelets on graphs. Example 1 shows that our construction is similar to the classical Haar wavelet. We can get framelets with other properties if we change \mathbf{p}_Λ and \mathbf{B}_Λ due to the flexibility guaranteed in Theorem 3.1.

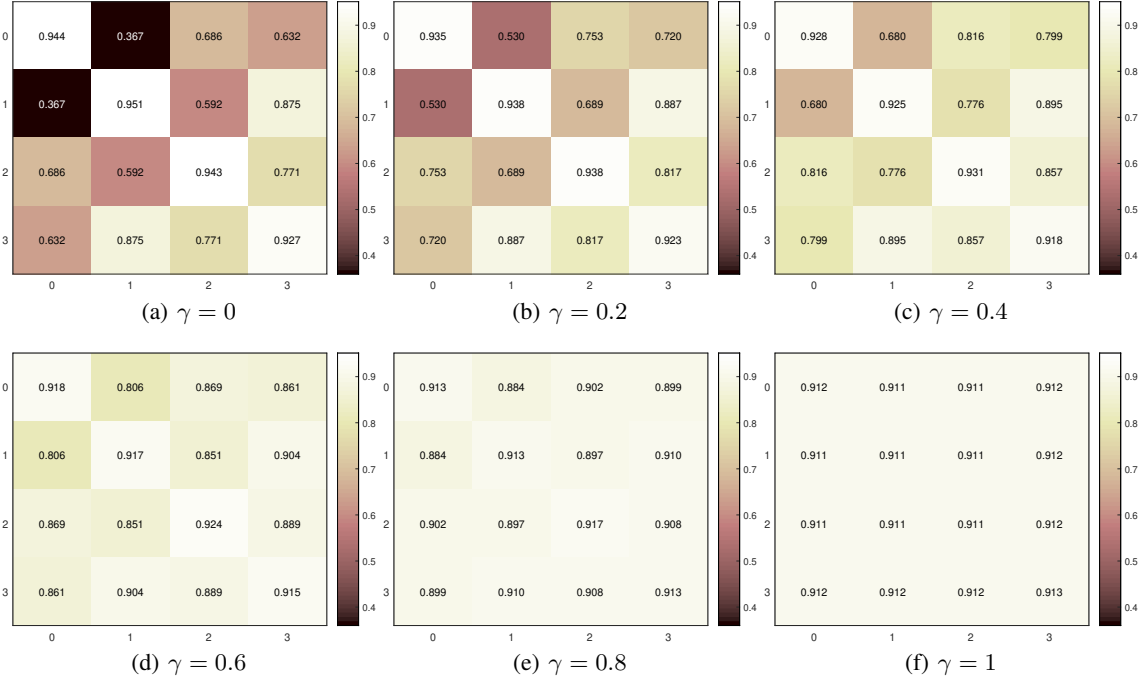
D Experiment Details on the Synthetic Dataset

[21] gives a theoretical characterization of graphs on which GCN fails to produce acceptable performance. We follow and modify Algorithm 2 in [21] to generate synthetic data.

The key idea of the algorithm is to generate edges of nodes in a graph such that the intra-class and inter-class similarities are properly controlled. The intra-class and inter-class similarity are defined by Appendix D. Cross-class neighborhood similarity (CCNS) measures how close the patterns of connections of nodes between two classes are. In our experiment, we generate graphs with 3000 nodes for which assign labels from $\mathcal{C} = \{0, 1, 2, 3\}$ randomly. It means that we have $n_c = 4$ classes. We generate edges according to Algorithm 4. The distributions that control CCNS are designed based on the uniform distribution and a prescribed distribution $\{\mathcal{D}_c : c \in \mathcal{C}\}$. The distributions $\{\mathcal{D}_c : c \in \mathcal{C}\}$ can be found in Table 5. Integer K is set to be 45000. The hyperparameter $\gamma \in \{0, 0.2, 0.4, 0.6, 0.8, 1\}$ indicates the probability to sample neighbors from uniform distribution other than the predefined distributions that are much more distinguishable for different classes. When γ is small, vertices of the neighborhood are more likely to be sampled according to $\{\mathcal{D}_c : c \in \mathcal{C}\}$ and when γ is large, it is more likely to sample from the indistinguishable uniform distribution. As a result, when γ becomes larger, the uniform distribution has more impact on CCNS and thus the metric becomes more similar between classes. We evaluate CCNSs on the generated graphs and show heatmaps in Figure 7. As we can seen, when $\gamma = 0$, CCNS is dominated by $\{\mathcal{D}_c : c \in \mathcal{C}\}$, and since \mathcal{D}_0 is more similar to \mathcal{D}_2 than \mathcal{D}_1 , we get $s(0, 1) = 0.367 \leq 0.686 = s(0, 2)$. And finally when $\gamma = 1$, all CCNS are almost 0.91. Notice that in Algorithm 4, we slightly modify the algorithm in [21]. Since we generate graphs with only nodes initialized, when $r \leq \gamma$, we sample label c from all labels \mathcal{C} , instead of $\mathcal{C} - \{y_i\}$ used in [21].

Definition D.1 (Cross-Class Neighbourhood Similarity (CCNS) [21]). Given graph \mathcal{G} and node labels $y_i \in \{0, 1, \dots, n_c - 1\}$ for $i \in \mathcal{V}$. the metric between classes c and c' is $s(c, c') = \frac{1}{|\mathcal{V}_c||\mathcal{V}_{c'}|} \sum_{i \in \mathcal{V}_c, j \in \mathcal{V}_{c'}} \cos\langle d(i), d(j) \rangle$, where $\mathcal{V}_c := \{i \in \mathcal{V} : y_i = c\}$ and $d(i) \in \mathbb{R}^{n_c}$ is a vector with elements defined by $\#\{j : (i, j) \in \mathcal{E}, y_j = c\}$ for any $c \in \{0, 1, \dots, n_c - 1\}$.

Features on graph nodes are from \mathbb{R}^{700} , with each elements randomly generated according to Gaussian distribution $(-\frac{9}{2} + \frac{1}{2}c)\xi$ independently, where $\xi \sim N(0, 1)$ and c is the label.

Figure 7: CCNS on the synthetic graphs with different hyperparameters γ .**Algorithm 4** [21]

Input: Nodes \mathcal{V} , Integer K , Distribution matrix $\{\mathcal{D}_c : c \in \mathcal{C}\}$, labels $\mathcal{C} = \{c\}_{i=0}^{n_c-1}$, γ
 initialize $\mathcal{E} = \emptyset$ and $k = 0$;

while $k \leq K$ **do**

 Sample $i \in \mathcal{V}$ and $r \in [0, 1]$ uniformly

 Obtain the label $y_i \in \mathcal{C}$ of node i

if $r \leq \gamma$ **then**

 Sample a label c from \mathcal{C} uniformly
else

 Sample a label c from \mathcal{C} according to distribution \mathcal{D}_{y_i}

 Sample node j from class c uniformly

if $(i, j) \notin \mathcal{E}$ **then**

 update $\mathcal{E} \leftarrow \mathcal{E} \cup (i, j)$
 update $k \leftarrow k + 1$

Output: $\mathcal{G} = (\mathcal{V}, \mathcal{E})$

E Experiment details of forming hierarchical partitions

We constrained the clusters to have no more than 4 nodes in each clustering step. Once new partition \mathcal{V}'' of clusters is formed from a graph $G' = (\mathcal{V}', \mathbf{A}')$, we define as follows the new adjacency matrix \mathbf{A}'' to form the graph

$\{\mathcal{D}_c : c \in \mathcal{C}\}$	class 0	class 1	class 2	class 3
\mathcal{D}_0	0.1	0.4	0	0.5
\mathcal{D}_1	0.5	0	0.5	0
\mathcal{D}_2	0.2	0	0.5	0.3
\mathcal{D}_3	0.25	0.25	0.25	0.25

Table 5: Distribution D_4 .

$G'' = (\mathcal{V}'', \mathbf{A}'')$ for next level clustering:

$$\mathbf{A}_{ij}'' = \sum_{p=1}^{n'} \sum_{q=p+1}^{n'} \mathbf{A}'_{pq} \delta(ID(p), i) \delta(ID(q), j),$$

where $\#\mathcal{V}' = n'$, $\#\mathcal{V}'' = m'$, $ID(p)$, $ID(q)$ are the indices of clusters that nodes p and q belong and $\delta(a, b)$ takes 1 when $a = b$. For heterophilous graphs, we iterate for a few steps until the final graph had less than 4 nodes. For *Pubmed*, we constrained the number of steps of generating hierarchical clustering to be exactly 6. The constant 4 and 6 are related to h and K in Theorem 3.9, which shows that when we use the binary Haar graph Haar framelets, the total number of framelets only linearly increases with respect to the total number of nodes in the graph. In practice, this gives acceptable numbers of generated framelets for the datasets.